Evaluation of the ALMA Prototype Antennas

Executive Summary

**Jeff Mangum (NRAO), Jaap Baars (ESO),
Albert Greve (IRAM), Robert Lucas (IRAM),
Ralph Snel (Lund University), Pat Wallace (RAL)**

May 28, 2004

Contents

Chapter 1

Introduction

The two ALMA prototype antennas are located at the site of the VLA in New Mexico. The evaluation of the antennas has been carried out by the Antenna Evaluation Group (AEG), consisting of experienced "antenna testers" from both organizations, AUI/NRAO and ESO. The charge of the AEG was to subject both antennas to a series of identical tests which would indicate the compliance (or not) of the antennas with the specifications. Because of the sensitive nature of the evaluation with respect to the contractors, the AEG has been bound to strict confidentiality with regard to the dissemination of the results. Only the ALMA Management has been kept informed about the progress in and results of the evaluation.

The core of the AEG is composed of the authors of this executive summary to the ALMA Management. We have been assisted in various stages of the evaluation by our colleagues José Lopez Perez of OAN (Spain), Henry Matthews of HIA (Canada), Angel Otárola of ESO, Michael Bremer of IRAM (France), David Smith (MERLAB), Mark Holdaway, Nicholas Emerson, Jack Meadows, and Fritz Stauffer of NRAO, and the VLA Mechanical Workshop. We also acknowledge assistance from members of the NRAO and ESO antenna teams and the NRAO electronics and computer divisions.

In this report we present an executive summary of our evaluation efforts. After a very short description of the antennas, the major specifications to be tested and the limitations of our methods and apparatus, we summarize the results of our evaluation for both antennas, separated into sections concerning the major specifications. In accordance with our charge, we refrain from presenting a comparative judgment and limit ourselves to the presentation of measured data and their analysis.

Chapter 2

Antenna Layout and Main Specifications

2.1 Basic Antenna Layout

The ALMA antennas are alt-azimuth mounted Cassegrain dual-reflector systems of 12 m diameter with a reflector surface and pointing accuracy suitable for observations in the 0.3 mm submillimeter band. VertexRSI delivered an antenna to AUI/NRAO and ESO obtained an antenna from the consortium Alcatel/EIE (AEC). A picture of the two antennas is shown on the cover of this report. The main characteristics of the antennas are summarized in Table 2.1.

2.2 Major Specifications

It has been the main task of the AEG to establish the compliance of the ALMA prototype antennas with the following major specifications:

- Reflector Surface Accuracy: **25μm with 20μm goal**
- Absolute Pointing Accuracy: **2 arcsec over all sky**
- Offset Pointing Accuracy: **0.6 arcsec over 2° radius**
- Fast Switching: **1.5° move in 1.5 sec, settle to 3 arcsec peak pointing error**
- Path Length (Non-Repeatable): **15μm**
- Path Length (Repeatable): **20μm**

These specifications must be satisfied under all attitude angles of the antenna and all environmental situations, in particular wind of 6 m/s (day) and 9 m/s (night) as well as full solar illumination from changing directions.

Table 2.1: Main Properties of the ALMA Prototype Antennas

Property	**VertexRSI**	**Alcatel/EIE (AEC)**
Base/Yoke/Cabin	Insulated Steel	Steel/Steel/CFRP
BUS	CFRP, 24 sectors, open back, covered by removable GFRP sunshades	CFRP, 16 sectors, closed back sectors glued and bolted together.
Receiver Cabin	Cylindrical Invar/Thermally-Stabilized Steel	CFRP; Direct connection cabin to BUS
Base	3-point support - bolt connection with foundation	6-point base support - flanged attachments
Drive	Gear and Pinion	Direct drives on both axes with linear motors
Brakes	Integrated on servo motor	Hydraulic disk brakes
Encoders	Absolute (BEI)	Incremental (Heidenhain)
Panels	264 Panels, 8 rings, machined AL, open back, 8 adjusters (3 lateral/5 axial) per panel	120 Panels, 5 rings. AL-honeycomb core with replicated Nickel skins, Rhodium coated. 5 adjusters per panel
Apex/Quadripod	CFRP structure, + configuration	CFRP structure , $\times$ configuration
Focus Mechanism	Hexapod (5 DOF)	Three axes (x,y,z) mechanism
Total Mass	$\sim$ 108 tonnes	$\sim$ 80 tonnes
Mass Dist (El/Az)	50%/50%	35%/65%

Chapter 3

Limitations of the Evaluation

Unfortunately, large delays in the delivery of the antennas have not enabled us to carry the evaluation to a point where a number of the performance specifications could be extensively evaluated. The Vertex antenna was marginally put at our disposal in March 2003, the AEC antenna in January 2004. Neither antenna was fully functional at those times. The evaluation of the antennas has been limited by the atmospheric conditions available, the capabilities of the available measurement devices, and most importantly the time allowed for the evaluation activities. Specifically, our ability to measure the full performance of the prototype antennas has been limited in the following areas:

1. Reflector surface deformation as function of elevation. The holographic surface measurement is limited to one elevation angle.

2. Wind performance has been studied but only to the extent that strong winds were available at the site.

3. Radiometric pointing measurements are the final criterion for the determination of the pointing behaviour. The system temperatures of the evaluation receivers are excellent; however the limits set by gain fluctuations were factors of order 20 (at 3mm) and 10 (at 1mm) above the thermal fluctuations. Thus our limiting sensitivity has been entirely set by gain stability at the 10 Hz switching frequency, restricting the number of available sources to ~ 20 at 3mm wavelength. The nutator could only operate reliably under quiet or moderately windy conditions (a few m/s). Only a limited set of data could be collected at the VertexRSI antenna, and even less on the AEC antenna.

4. Climatic conditions at the VLA site are not representative of the final Chajnantor site. In particular the atmospheric transmissivity is only sufficiently good for observations at the longer mm-wavelengths and over a limited (winter) period of the year. This has significantly impeded the quantity and quality of the radiometric tests.

5. It has become clear that the VLA site has poor seeing–seldom better than 4 arcsec. With the OPT's 100 mm aperture, the seeing manifests itself as large and rapid movements of the image, making optical measurement of the all–important tracking and offsetting performance difficult.

6. The comparatively short focal length of the optical pointing telescope (OPT) means that the image is under–sampled, and in some of the tracking tests quantization effects are evident. These effects make performance limitations much below 1 arcsec difficult to detect. It is far from obvious how this design could have been made better. Deliberate defocusing was used to ameliorate the position undersampling and longer exposure times to average out the seeing.

7. The lack of easy access to the finite element model for the VertexRSI antenna was a major encumbrance to the evaluation process.

8. Specifications outside our specific charter, including:

   (a) Time needed to remove and attach the antenna to its foundation.

   (b) Alignment errors after a drop of the antenna during transportation.

   (c) Mechanical and electrical requirements. These were verified by the Antenna IPT during acceptance testing.

Chapter 4

Performance At-A-Glance

4.1 Overall Conclusion of the Evaluation

The overall performance of the ALMA prototype antennas within the primary performance specifications is summarized in Table 4.1. To supplement this table, we note that:

1. The grade "Provisionally Meets Specification" means that with a reasonably complete set of measurements we find that the antenna nearly meets the specification, and shows no apparent flaws which would lead to an absolute violation of this specification.

2. The grade "Provisionally Fails to Meet Specification" means that with a reasonably complete set of measurements we find that the antenna nominally fails to meet the specification. Furthermore, the suspected mode of failure suggests a potential hardware deficiency which, when not corrected, would lead to an absolute violation of this specification.

3. All metrology systems, in their state of operation during our evaluation, on the two prototype antennas were unsuccessful at improving the pointing performance of the antennas. In a final, well working state these systems might still bring an improvement.

4. The provisional failure of the AEC antenna to meet the all–sky pointing specification may be due to an instability in the azimuth bearing. Superimposed on repeatable and readily modeled effects are random variations in both elevation and in Az/El nonperpendicularity. These random errors were seen to compromise the offset pointing performance for fields at high elevations where the offsets produce comparatively large azimuth changes.

5. Our measurements suggest that the VertexRSI antenna meets the offset pointing specification. This conclusion is provisional given the difficulties of measuring systematic errors at these accuracies.

6. The all–sky pointing specification allows for a recalibration of the pointing model only once a month. Since this specification must be consistent with the offset pointing

ALMA Prototype Antenna Performance Summary

Parameter	VertexRSI	AEC
Surface	M	M
Pointing (All-Sky)	PM	PF
Pointing (Offset)	PM	PM
Fast Switching	PM	M
On-The-Fly	M	M
Path Length	M	M

M $\equiv$ Meets specification

PM $\equiv$ Provisionally meets specification

PF $\equiv$ Provisionally fails to meet specification

specification, which allows for a recalibration every 15 minutes, updates to some fraction of the pointing model are allowed on this timescale. The performance of both antennas within this poorly–conceived specification has shown that:

(a) With no metrology correction, the VertexRSI antenna requires a recalibration of the two collimation and the two azimuth axis tilt terms of its pointing model to meet the specification. However, if the tiltmeters in the base of the VertexRSI antenna are functioning correctly this should take care of azimuth axis tilt term recalibration in real–time, leaving only the two boresight terms to be recalibrated routinely.

(b) With no metrology correction, the AEC antenna warrants only a recalibration of the two collimation pointing terms, as allowing any of the other geometric pointing model terms to vary does not lead to appreciable improvement. Even with this recalibration the AEC antenna still provisionally fails to meet the specification.

7. The positioning servo of the AEC antenna seems to be very well tuned, showing little overshoot for most antenna motions.

8. Even though the time baseline for such a characterization is limited, the pointing model for the AEC antenna appears to be quite stable over timescales longer than one month.

9. The VertexRSI apex seems to rotate about the boresight axis, with negligible offset between the rotation and boresight axis. The AEC apex has an offset of the rotation axis of order one centimeter, varying with elevation. The AEC apex structure is 3–4 times less stiff for boresight rotation than the VertexRSI apex structure. The offset of the AEC apex rotation axis, combined with the relatively large rotation causes a displacement component of the apex structure, which would result in motion of the secondary focus. The effect is large enough to affect radiometric pointing (though not compromising the specification), and to shake the BUS in the cross-elevation direction. The coupling between apex motion and azimuth motion has been seen in many types of measurements, and has even caused the antenna to go into servo oscillation on repeated occasions.

In the following sections we summarize some general conclusions and comments with respect to both antennas. More details will be found in Chapters 5 and 6, where the major results for each of the two antennas will be presented.

4.2 Reflector Measurement and Setting Conclusions

1. The holography system has functioned according to specification and has enabled us to measure the surface of the antenna reflectors with a repeatability of $< 10\mu$m. Based on repeated measurements and our evaluation of the system, we estimate that the overall (systematic and random) error in the determination of the surface RMS value will not be larger than 5μm.

2. On the VertexRSI antenna we have achieved a surface accuracy of $< 20\mu$m RMS after five full and two partial panel settings. Note that all measurements were made with the receiver cabin temperature stabilization system active.

3. On the AEC antenna we have achieved a surface accuracy of 15μm RMS after two full and one partial panel settings.

4. The small differences in the surface maps obtained over several days of measurement are consistent with the measurement accuracy and are at worst marginally significant. If taken at face value, they indicate that the deformations of the reflector under varying wind and temperature influence are fully consistent with, and likely well within, the specification.

We have successfully performed a holographic measurement and consecutive panel setting of the reflectors of the two ALMA prototype antennas. The data collection and analysis software packages are easy to use and provide quick results of the measurements, directly usable for a panel correction setting. We consider this system suitable for the routine setting of the ALMA production antennas to the goal of 20μm accuracy in an acceptable time span. Modern survey equipment will enable the contractor to deliver the reflector with an accuracy of 50-60μm without undue effort. Although the holography system can easily start from a much larger error, in the former case it is feasible to reach the specification with only a few panel settings based on holography. We propose that this be done with all production antennas at the OSF.

In conclusion we can state that the reflectors of both antennas behave equally well. The specification and goal have been met. The variations in surface RMS, measured over time and under changing environmental conditions, are equally small for both antennas. They are well within the range allowed by the specification and consistent with our measurement accuracy. This excellent behaviour over time is more important than the actually achieved surface setting. We stopped iteration of the settings after having achieved the goal of less than 20μm. Without the small remaining effect of some offset in the data for the outer part of the VertexRSI antenna (see §5.1.1), the final result would probably have been several microns smaller, similar to that achieved on the AEC antenna.

4.3 Pointing Measurement Conclusions

1. All–Sky Pointing

   (a) Even without the metrology inputs the all–sky pointing derived from optical measurements just meets specification for the VertexRSI prototype antenna.

   (b) The AEC prototype antenna falls short of the 2 arcsec all–sky pointing specification, averaging at 2.25 arcsec RMS (OPT measurements). The erratic cross-elevation performance, perhaps due to variations in azimuth/elevation non-perpendicularity arising from instability in the azimuth bearing, means that although some tests have delivered within–spec performance, most have not. If allowance is made for the intrinsic noise level of the measurement process

the average performance approaches specification. However, there are certain regions of sky (at high elevations and certain azimuths) where the performance is always out of specification.

(c) The VertexRSI radiometric tests are too few and limited in sensitivity to measure the actual all–sky pointing accuracy. It is undoubtedly better than ~ 4 arcsec but repeatable azimuth drifts are clearly detected, at the level of ~ 0.7 arcsec/hour (possibly due to ambient temperature drifts of order 1.4 K/hour, over a period of several hours).

(d) Radiometric measurements of the AEC antenna are too few and limited in sensitivity to measure the actual all–sky pointing accuracy, but there are indications that it is between 3 and 4 arcsec RMS. Drifts at the 1 arcsec/hour level were marginally detectable on some runs.

(e) Accelerometer measurements indicate that for timescales of several seconds, the absolute pointing performance of 2 arcsec is not in danger due to pointing jitter of the BUS for either antenna.

2. Offset Pointing

(a) Verification of the offset pointing specification has been difficult to verify using optical pointing measurements. Whether the 0.6 arcsec specification is being met with the VertexRSI antenna is difficult to guarantee, but there is no evidence that it is not.

(b) Tests of the offset pointing performance of the AEC prototype antenna showed systematic pointing differences between the respective stars used that slightly exceeded the 0.6 arcsec specification. The field concerned was fairly close to the zenith (between 20 deg and 8 deg away) and this behaviour is presumably a manifestation of the suspected azimuth bearing instability that is suggested by the all–sky tests.

(c) Radiometric measurements of the offset pointing performance of the VertexRSI antenna are clearly dominated by atmospheric seeing. Experiments where we switched between the half power point on Jupiter and a position 1.5 degrees away show a RMS of 0.6 arcsec per axis, or 0.8 arcsec total, when the antenna is settled (after 2.5 seconds).

(d) Radiometric measurements where we switched the AEC antenna between the half power-point on Jupiter and a position 1.5 degrees away show very small radiometrically determined errors that are limited by the 5Hz oscillation at a level of 0.4 arcsec peak-to-peak when the antenna is settled.

(e) Radiometric measurements using the VertexRSI antenna, where the half–power points of Jupiter were continuously tracked under low-wind conditions over a period of several minutes, show azimuth encoder errors of ~ 0.25 arcsec RMS, and elevation encoder errors of ~ 0.44 arcsec RMS. The radiometrically measured pointing errors are much larger (~ 0.68 arcsec and ~ 0.95 arcsec). There is very convincing evidence however that the difference is entirely of atmospheric origin (the radiometer noise contributes only ~ 0.2 arcsec RMS).

(f) Radiometric measurements using the AEC antenna, where the half–power points of Jupiter were continuously tracked under low–wind conditions over a period of several minutes, show encoder errors at a level of 0.03 arcsec RMS on both axes (0.041 arcsec total). The radiometrically measured pointing errors are larger, at the 0.6 arcsec level, and are of atmospheric origin.

(g) Accelerometer measurements of the RMS BUS pointing jitter during sidereal tracking under windy conditions indicate that the AEC antenna is well within specification. For the VertexRSI antenna, the 0.6 arcsec specification is only met after scaling the wind and pressure conditions to those specified for Chajnantor, and averaging over many azimuth/elevation combinations. For sidereal tracking low in the southeast and southwest, the antenna BUS jitter is near 0.6 arcsec already for low wind conditions. Addition of wind induced pointing jitter raises the overall BUS RMS pointing for these orientations and primary operating conditions to a value above 0.6 arcsec.

(h) Accelerometer measurements indicate that during primary operating conditions the offset pointing errors for the BUS are dominated by tracking errors on the VertexRSI antenna. Wind effects dominate pointing stability for the AEC antenna, while remaining well within the specification for timescales of 4 seconds or shorter.

4.4 Fast Switching Evaluation Conclusions

We had four independent channels of data through which we could evaluate the prototype antennas' fast switching capability:

1. Optical pointing offsets, in which the fit positions of a star on the optical telescope's CCD, or deviations from the star's mean position, infer the antenna's motion on the sky,

2. Radiometric pointing offsets, in which pointing information for a single axis at a time (Az or El) can be inferred from total power fluctuations when a bright source is observed near the half power point in the radiometric beam,

3. Antenna encoder readings, and

4. Accelerometer measurements.

Optical pointing offsets will be contaminated by atmospheric fluctuations which will have characteristic time scales shorter than our 0.1 s integration time, radiometric pointing offsets will be contaminated by atmospheric fluctuations with characteristic time scales of about 1 s, and we do not know *a priori* that the encoder readings accurately represent the motion of the radiometric beam on the sky. For technical/scientific reasons, we were unable to get optical pointing data and radiometric pointing data simultaneously, but of course, we were able to get encoder data whether we were performing optical pointing observations or radiometric pointing observations. Utilizing at least three of the available observational tools listed above, we find that:

VertexRSI:

1. The VertexRSI prototype antenna was studied using all four techniques. From our radiometric measurements, which represent the most direct of the fast switching performance measurements, we find that the source is reached (to within 3 arcsec) about 1.7 s after the start of the fast switching slew, and the *mean* Az pointing error after the antenna is on source is very small (typically less than 0.5 arcsec). The *RMS* pointing error for the last half of this scan is much larger, about 0.8 arcsec in each axis, but this includes atmospheric contributions.
2. The optical and simultaneous encoder data paint a similar picture of the fast switching performance of the VertexRSI prototype. The antenna takes about 1.8 seconds to get from one source to another source 1.77 degrees away with 2 arcsec pointing errors. After 3 seconds, the pointing errors decrease substantially; at this level, the atmosphere contributes appreciably to the pointing errors.
3. The data indicate there is a slap-back/overshoot problem with the azimuth servo system between 2 and 3 s into the slew. (Some slew geometries show an overshoot, and some show a slap-back.) We assume that tuning the servo system could essentially eliminate this problem.
4. The accelerometer measurements indicate that the settling time to within 3 arcsec depends on the azimuth, elevation, and switching direction. For some directions, settling time is approximately 1.5 seconds, while for other conditions, an additional second may be needed to reach 3 arcsec pointing accuracy. After approximately 2.5 seconds, pointing has stabilised to a level which does not differ significantly from the RMS pointing stability, which is approximately 0.4 arcsec.

AEC:

1. The AEC prototype antenna was also studied using all four measurement techniques. Based on the radiometric measurements, we find that the source is reached with 3 arcsec accuracy about 1.5 s after the start of a slew, about 1 arcsec after 1.8 s, and under 0.2 arcsec RMS after 2 s.
2. A 5 Hz mechanical pointing oscillation is excited by fast switching antenna motions, but this oscillation has a peak to peak amplitude of 0.4 arcsec or less, damps out after several seconds, and is not seen in tracking data (only when the antenna is abruptly started and stopped as in fast switching).
3. From an analysis of the encoder pointing errors, we find that for fast switching slews between two sources 1.76 deg apart the AEC antenna gets on source within the 3 arcsec fast switching pointing specification between 1.3 and 1.4 s, and has RMS pointing errors of under 0.5 arcsec for 1.6 s after the start of the slew. The fast switching slew is very clean, and the servo system seems to be very well-tuned to this sort of antenna motion.
4. Based on accelerometer measurements, during fast switching, the AEC antenna experiences no visible overshoots in azimuth and elevation pointing, with the exception of some sub–arcsecond resonances, mostly in elevation, which damp out after a few seconds. Settling time to within 3 arcsec is under 1.5 seconds, for small pointing offsets. After approximately 3 seconds, pointing has stabilised

to a level which does not differ significantly from the RMS pointing stability, which is below 0.1 arcsec.

4.5 On-The-Fly Evaluation Conclusions

Our only means for measuring the On-The-Fly (OTF) performance of the prototype antennas was to compare the commanded and actual encoder positions of the antenna while executing OTF patterns. The OTF mapping performance is driven by the maximum velocity and acceleration performance of the antenna. By conducting simulated total power and interferometric OTF observations while sampling the position information sent to and from the antenna, we find that:

1. The VertexRSI antenna meets the OTF performance specifications, assuming a reasonable allowance for observing pattern efficiency.

2. The AEC antenna meets, and in many ways exceeds, the MOTF performance specification, but shows some anomalous azimuth tracking for TPOTF measurements at the highest scan velocity. We suspect that this anomaly is a contractor software error which is solvable.

4.6 Path Length Evaluation Conclusions

A direct measurement of the full path length variation, for instance between the Cassegrain focus and the ground, is not possible. The path length variation of several sections of the antennas (pedestal, fork arm, quadripod) have been measured and monitored, and from these measurements the full path length variations have been inferred.

1. For both prototype antennas we find that the full path length is expected not to vary by more than $\sim 15-20\mu$m within about 30 minutes of time. For time intervals longer than ~ 30 minutes, the path length variation of the steel components (pedestal, fork arms) start to show the influence of the daily temperature variations of the ambient air and of solar irradiation of the associated thermal dilations of the steel. The long-term path length variations of the dominant steel components of the antennas, which may amount to $\sim 100-200\mu$m within 24 hours, can be predicted from temperature measurements at a few selected positions (for instance selected from available FEM calculations).

2. For both antennas, the variation of the L2 path length for time intervals of 30 minutes can be explained by the daily sine-like ambient air temperature variation and a correspondingly sine-like induced thermal dilation of the fork arm(s).

3. For both antennas we find that the full path length variation is within the specification under movements of the antennas, *i.e.* sidereal tracking, on-the-fly mapping, and fast switching operation.

4.7 Focus Evaluation Conclusions

1. For the VertexRSI antenna, there is good agreement between the measured photogrammetric, quadrant detector, API5D, and radiometric focus values.

2. The difference between the FEM and the measurements of the VertexRSI antenna suggests that the BUS is slightly less stiff and the quadripod more stiff than that predicted by FEM.

3. From the radiometer and holography measurements on both prototype antennas, we have derived the change in best-fit focal length of the primary reflector as a function of temperature. On the VertexRSI prototype antenna a change of 36μm/C is measured, while on the AEC antenna a change of 20μm/C is measured. These cause path length errors in excess of the specification. Note however that this is a highly repeatable error which will be almost the same for all antennas in the array. By measuring the temperature it can be quite accurately corrected, if desired.

4. The difference of the FEM and measurements of the AEC suggest that the BUS is stiff and that the quadripod is less stiff than predicted by the FEM.

Chapter 5

Evaluation Results for the VertexRSI Prototype Antenna

5.1 Surface Accuracy Performance

5.1.1 Holography

The reflector surface accuracy specification requires the VertexRSI antenna to have a surface accuracy of 20μm. ALMA has assumed the task to demonstrate this with the aid of a holography system at 3 mm wavelength. The initial surface setting was performed by VertexRSI with digital photogrammetry to 85μm. The holography system was designed to provide a measurement repeatability of $< 10\mu$m.

The first holographic measurements of the VertexRSI antenna indicated that the focus of the best-fit paraboloid set by the contractor was misplaced relative to the holography signal feed by $\sim$ 5mm in X and Y. As the mounting of the holography signal feed was well-centered at the mechanical prime focus position, we removed this focus offset with first panel setting.

Subsequent measurements allowed us to reach a surface RMS of less than 20μm after 5 settings of the surface. At the end we made numerous surface maps over several days to study any influence of the changing environmental conditions. None could be found with any significance. In Figure 5.1 the time series of a number of measurements is shown, indicating the high stability of the surface over time.

With increasing accuracy the presence of an artifact in the data for the outer area of the aperture became apparent. The effect can be described by a DC-offset in the central point of the measured antenna map, *i.e.* some saturation on the point with the highest intensity. This artifact is clearly *not* a feature in the antenna structure. By adjusting this offset in the software, most of the artifact could be removed. This has been done with the final data analysis.

The adjustments were performed with a simple home-made tool. Two people on a man-lift approached the surface from the front, where the adjustment screws are located. The time needed for an adjustment of the total of 1320 adjusters was 8 hours, which is the specified maximum time.

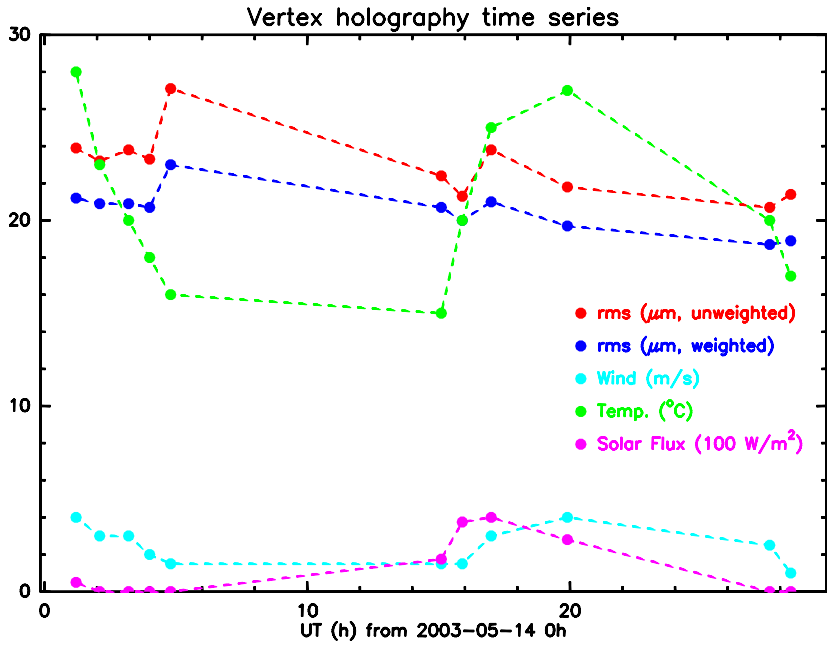

Figure 5.1: Time series of the holography of the VertexRSI antenna over a period of two days in May 2003. The weighted (applying the illumination function, taper) and unweighted RMS values are given along with temperature, wind speed and solar flux. There is no discernible influence of the varying environmental parameters on the RMS values.

5.1.2 Temperature Sensor Measurements

The analysis of several days of temperature monitoring of the BUS (24 sensors) shows that the BUS follows closely the variation of the ambient air temperature. The temperature homogeneity of the BUS over 24 hours is $\sim \pm 3$ K (PTP). The BUS is thermally stable and expected not to degrade the surface RMS value above the values predicted from the FEM (5 μm/K).

5.1.3 Radiometric Beam Maps

At the relatively long wavelengths available ($>$ 1mm) it is not really feasible to characterize the antenna surface by means of beam shape measurements. We have been able to make clean maps of Mercury (Figure 5.2). The first sidelobe level is $< 3\%$, and the beam size is 25 arcsec. From this measurement we cannot set a significant limit to large scale surface errors.

5.2 Pointing Performance

5.2.1 Optical Telescope and Radiometric Measurements

1. The pointing model constants determined by optical and radio means agree well together, when the gravitational bending of the backup structure, to which the optical

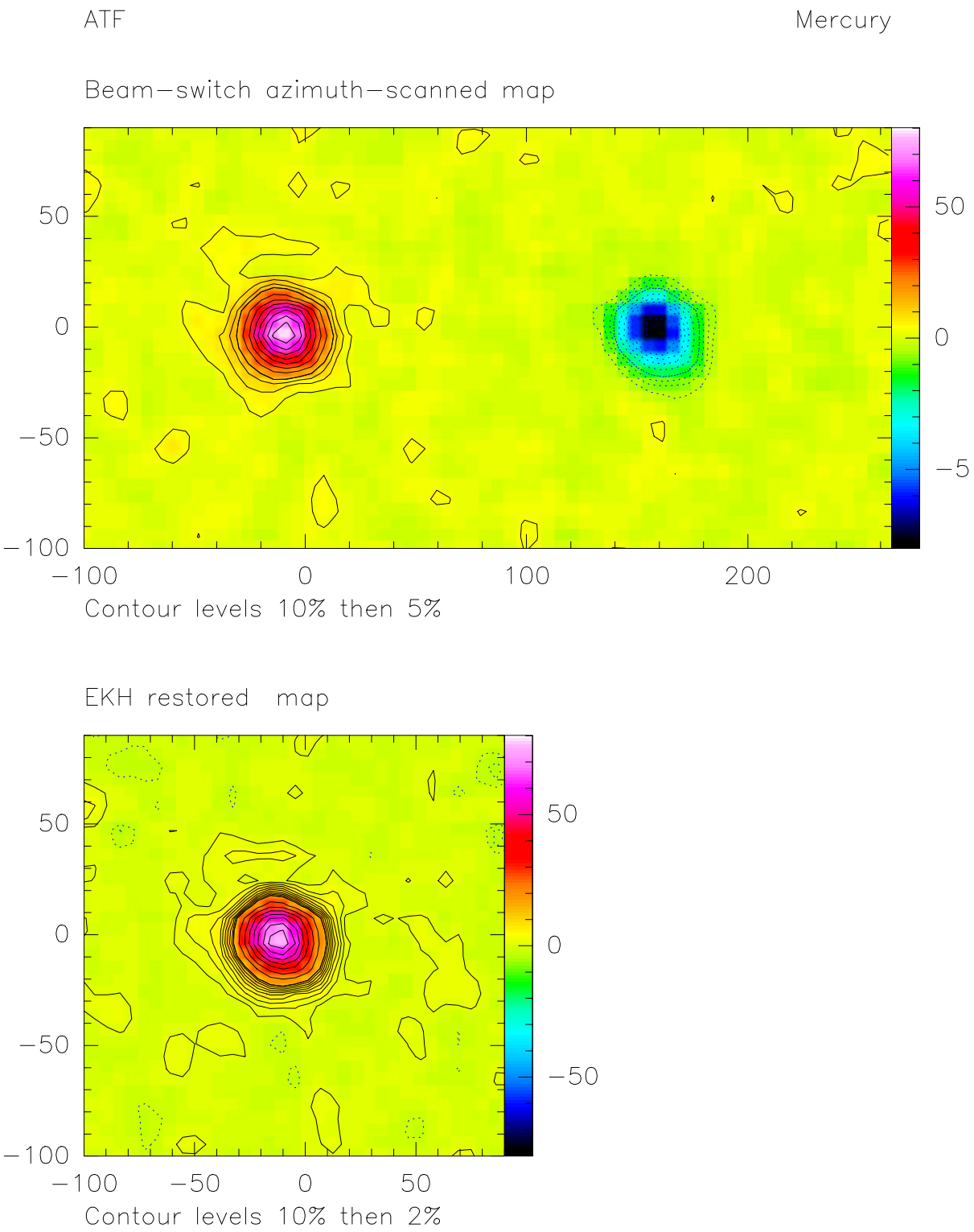

Figure 5.2: Planet Mercury observed at 265 GHz: angular distance from the Sun was 16 degrees; the planet angular diameter was 5.1 arcsec; contour levels are $5, 10, 20..., 90\%$. Top: raw beam-switched map (beam separation 160 arcsec); bottom: map restored with the EKH algorithm; contour levels are $2, 4, ..., 16, 18, 20, 30, ..., 90\%$. The low-level structure located ~ 35 arcsec north of the source in both the unrestored and restored maps is due to a slight defocus in the Y-coordinate.

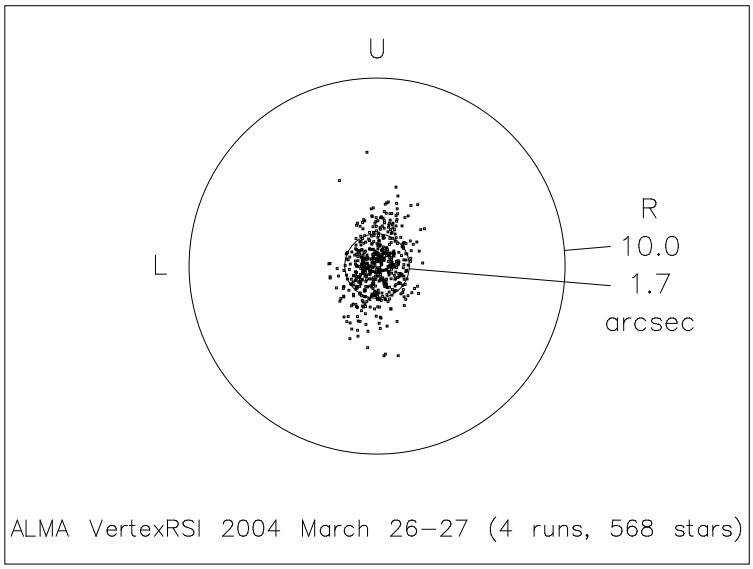

Figure 5.3: A good but representative all–sky optical pointing result for the VertexRSI prototype antenna. The 568 observations span nearly 24 hours and have simply been concatenated. The only adjustment that has been applied to the raw data is the removal of small drifts totaling less than 1 arcsec horizontally and 1.5 arcsec vertically. The pointing model used consists of a fixed core of ten simple correction terms, that applies to all the VertexRSI OPT runs, with a further five terms (encoder and boresight offsets plus mount tilt) that are fitted to each individual run.

telescope is attached, is taken into account. Due to the location of the telescope (horizontally displaced from the center of the reflector), this elevation-dependent bending has components both in azimuth and in elevation.

2. All-Sky Pointing

   (a) Even without the metrology inputs the all–sky pointing derived from optical measurements meets specification (see Figures 5.3 and 5.4).

   (b) Apart from large jumps in some coefficients which were the result of mechanical changes, the pointing model was fairly stable over the duration of the evaluation. The azimuth zero-point IA meandered somewhat but rapid variations were within ±2 arcsec. The elevation zero/boresight term was more noisy, perhaps ±10 arcsec, with the left-right boresight stable to about half that figure. (Some of this variation may be a consequence of the problems with the metrology systems.) The tilt terms, AN and AW, were both stable at the ±3 arcsec level. On many occasions, a whole sequence of pointing runs could be concatenated and reduced *en bloc* (*e.g.* Figure 5.3) , showing that recalibrations of the boresight and tilt terms with a handful of stars once or twice a day would probably be enough to maintain peak performance.

   (c) The all–sky pointing specification allows for a recalibration of the pointing model only once a month. Since this poorly–conceived specification must be consistent

with the offset pointing specification, which allows for a recalibration every 15 minutes, updates to some fraction of the pointing model are allowed on this timescale. To investigate this aspect of the all–sky pointing specification, we selected two good OPT all–sky data sets taken about a month apart. The first data set was used to fit the VertexRSI standard model, with the fixed core left at the nominal values. The sky RMS of this "operational model" was 1.54 arcsec. The second data set was fitted to the operational model, with only the boresight terms IE and CA allowed to vary, yielding a sky RMS of 3.05 arcsec. When the tilt terms AN and AW are allowed to vary, the sky RMS is an excellent 1.86 arcsec. It is clear from this (and other experiments) that tuning of all four of these terms will be needed in order for the VertexRSI antenna to meet the 2 arcsec all-sky specification. However, if the tiltmeters in the base are functioning this should take care of AN and AW, leaving only the two boresight terms to be recalibrated routinely.

(d) The radio tests are too few and limited in sensitivity to measure the actual all–sky pointing accuracy. It is undoubtedly better than ~ 4 arcsec but repeatable azimuth drifts are clearly detected, at the level of ~ 0.7 arcsec/hour (possibly due to ambient temperature drifts of order 1.4 K/hour, over a period of several hours).

(e) Over a total of 68 runs spanning about 5 months (but concentrated at the beginning and end of that period), the sky RMS was between about 1.5 arcsec and 3 arcsec. The high end of this range resulted from a faulty metrology system which produced aberrant residuals. In general, the scatter was usually between 50% and 100% larger in elevation than in cross-elevation. Figure 5.4 shows the sequence of optical pointing runs done since the introduction of improved test procedures in March 2004.

3. Offset Pointing

(a) The noise level from the short–term optical tracking and offsetting tests was typically 1.5 arcsec or less, at least as good as the all–sky optical pointing RMS results that have been obtained.

(b) A further conclusion, albeit more tentative, is that because the observed noise levels from the optical offsetting and tracking tests are the same, the offsetting is not adding significantly to the error. Whether the 0.6 arcsec specification (for offsets of 2° or less) is being met is harder to guarantee, but there is no evidence that it is not. For example on a 5–star field that was tracked from elevation 70 to 83 degrees, the largest displacement for an individual star compared with the mean was 0.3 arcsec with borderline statistical significance.

(c) The radiometric determination of relative pointing accuracy can be limited by atmospheric seeing, though at a lower level than for optical determination. From repeated measurements of Jupiter we obtained an upper limit of ~ 0.9 arcsec to the pointing repeatability. Experiments where we switched between the half

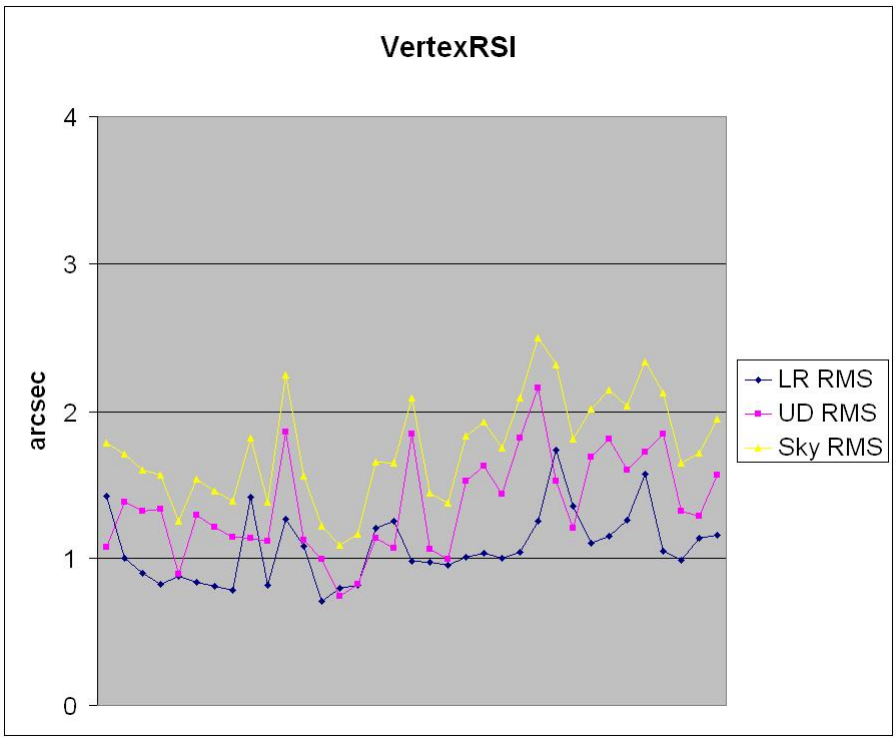

Figure 5.4: The all–sky optical pointing performance of the VertexRSI prototype antenna since the introduction of improved test procedures in March 2004. The horizontal axis is sequence number and not time. The elevation performance (the line labeled "UD RMS") is noticeably worse than the cross–elevation performance ("LR RMS") for reasons that are not understood and may be local optical seeing effects. Additional evidence that such local effects are playing a part is provided by the slow variation during the two months covered, suggestive of seasonal changes. Although a few tests fail to reach the 2 arcsec all–sky specification, most do, and if the better results are correlated with periods of more favorable weather the inherent antenna performance must be well below 1.5 arcsec RMS.

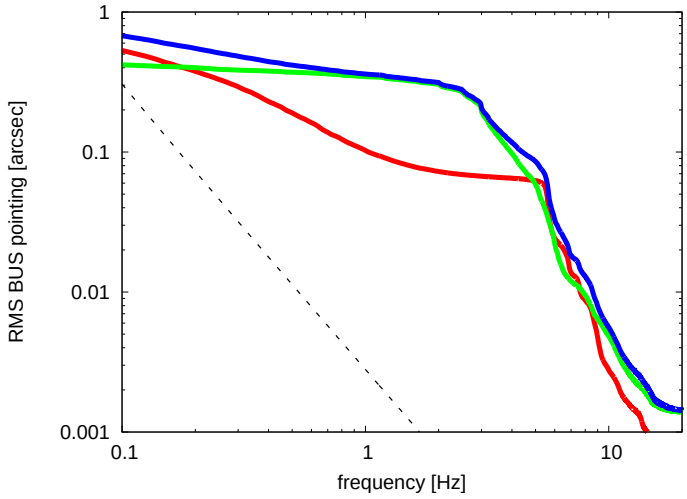

Figure 5.5: RMS BUS pointing and tracking stability for the VertexRSI antenna for 9 m/s wind at Chajnantor pressure. The red curve shows the effect of wind, without the effect of sidereal tracking. The green curve shows the effects of sidereal tracking for low wind conditions. The blue curve shows the combined effect of wind and sidereal tracking. The dashed line is an estimate of the noise in the blue curve. Each point in the curve shows the RMS pointing for that frequency and above, or alternatively over time periods corresponding to the frequency.

power point on Jupiter and a position 1.5 degrees away show a RMS of 0.6 arcsec per axis, or 0.8 arcsec total, when the antenna is settled (after 2.5 seconds).

(d) Experiments where we continuously tracked the half-power points of Jupiter under low-wind conditions over a time interval of 800 seconds show azimuth encoder errors of ~ 0.25 arcsec RMS, and elevation encoder errors of ~ 0.44 arcsec RMS. The radiometrically measured pointing errors are much larger (~ 0.68 arcsec and ~ 0.95 arcsec). There is very convincing evidence however that the difference is entirely of atmospheric origin (the radiometer noise contributes only to 0.2 arcsec RMS).

5.2.2 Accelerometer Measurements

For sidereal tracking under *low wind conditions*, the RMS all sky BUS pointing jitter over periods of 4 seconds is 0.39 ± 0.14 arcsec for the VertexRSI antenna. Wind performance as measured at the ATF (780 mbar pressure), scaled to 9 m/s average wind and 560 mbar pressure, following the weighting table in the Statement of Work, amounts to 0.33 ± 0.11 arcsec RMS over timescales of 4 seconds. This number excludes effects of sidereal tracking.

The combined wind and sidereal tracking performance of the BUS at timescales of 4 seconds, taking into account the pressure difference between the ATF and Chajnantor, amounts to 0.51 ± 0.18 arcsec. Figure 5.5 shows the RMS BUS pointing stability for the VertexRSI antenna for 9 m/s wind at Chajnantor pressure.

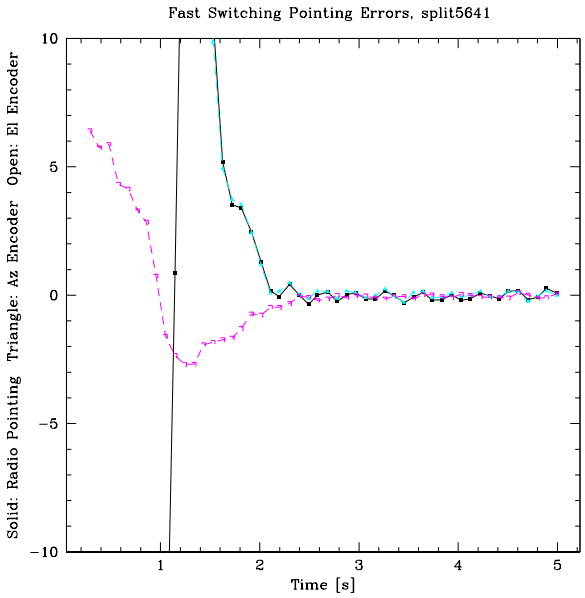

Figure 5.6: Radiometric fast switching measurement for the VertexRSI antenna. The mean radiometrically-inferred (solid black) and mean azimuth (cyan triangle) and elevation (purple dashed) encoder pointing errors as a function of time since the start of the 1.5 deg fast switching slew are shown. The source is reached with 3 arcsec pointing errors about 1.7 s after the start of the slew, and the *mean* AZ pointing error after 2.0 s is less than 0.5 arcsec.

5.3 Fast Switching Performance

5.3.1 Optical Telescope and Radiometric Measurements

Potentially, the most important information on fast switching comes to us from the radiometric tests, as that is the data which we will be most concerned with from the operational ALMA. By averaging over 20 fast switching approaches, we were able to get the random contributions of atmospheric pointing to average down in the radiometric data, and we found that the non–atmospheric component of the radiometrically–inferred pointing errors are well represented by the encoder pointing. The mean radiometrically–inferred and mean encoder pointing errors as a function of time since the start of the 1.5 deg fast switching slew are illustrated in Figure 5.6. The source is reached about 1.7 s after the start of the slew, and the *mean* Az pointing error after the antenna is on source is very small (typically less than 0.5 arcsec). The *RMS* pointing error (not shown) for the last half of this scan is much larger, about 0.8 arcsec in each axis, but this includes atmospheric contributions. This and other comparisons of the radiometric and encoder pointing measurements made with the VertexRSI antenna indicate that the encoders provide a fairly accurate assessment of the antenna pointing errors, not including any atmospheric contributions.

The optical and simultaneous encoder data paint a similar picture of the fast switching performance of the VertexRSI prototype. Figure 5.7 shows a typical optical fast switching measurement. The antenna takes about 1.8 seconds to get from one source to another

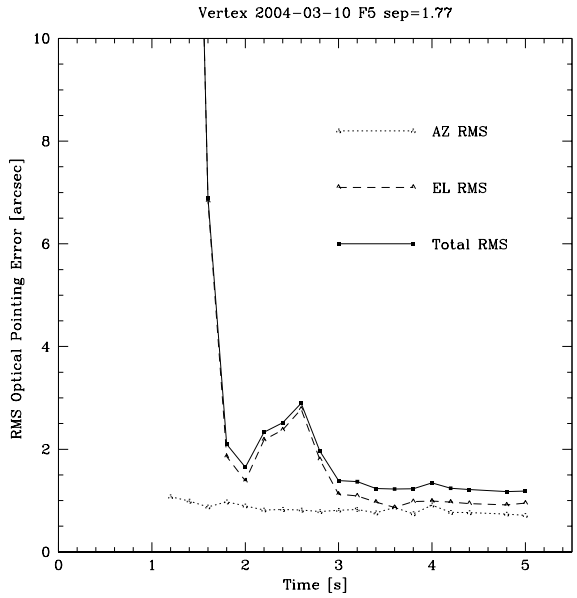

Figure 5.7: Example measurement of the RMS optical pointing offset as a function of time for the VertexRSI antenna. The mean pointing offset during the last half of each 5 s fast switching slew and settle cycle has been subtracted, and the RMS optical pointing is then calculated for all measurements that fall in a given time bin. A total of 5 minutes, or 56 slewing cycles were used to generate this plot. Embedded in these RMS pointing values are the results of the dry atmospheric fluctuations, or optical seeing, so the mechanical RMS pointing errors should be less than these values.

source 1.77 degrees away with 2 arcsec pointing errors. After 3 seconds, the pointing errors decrease substantially; at this level, the atmosphere contributes appreciably to the pointing errors. The data indicate there is a slap-back problem with the servo system between 2 and 3 s into the slew. (Some slew geometries show an overshoot, and some show a slap-back.) We assume that tuning the servo system could essentially eliminate this problem.

While the *mean* slewing profiles are needed to average down atmospheric effects and verify agreement between the radiometric and encoder data, it is really the *RMS* pointing errors that we are most interested in. As we saw in the optical data (which displayed the RMS pointing), we eventually become limited by the atmospheric fluctuations. Only the encoders will permit us to investigate the RMS pointing without being dominated by atmospheric effects. The RMS encoder pointing error as a function of time since the slew start for a fast switching slew of 1.77 deg is shown in Figure 5.8. (Note that these data were taken over the same time as the optical pointing data presented in Figure 5.7, and the similarities are obvious.) The encoder data indicates the antenna takes about 1.8 s to get on source, and it does so with a 2 arcsec RMS pointing error. After getting beyond the slap-back between 2 and 3 s into the slew, we achieve an RMS pointing error of about 0.5 arcsec, so the VertexRSI antenna will probably exceed the more demanding 0.6 arcsec specification for the last 2 s of the scan.

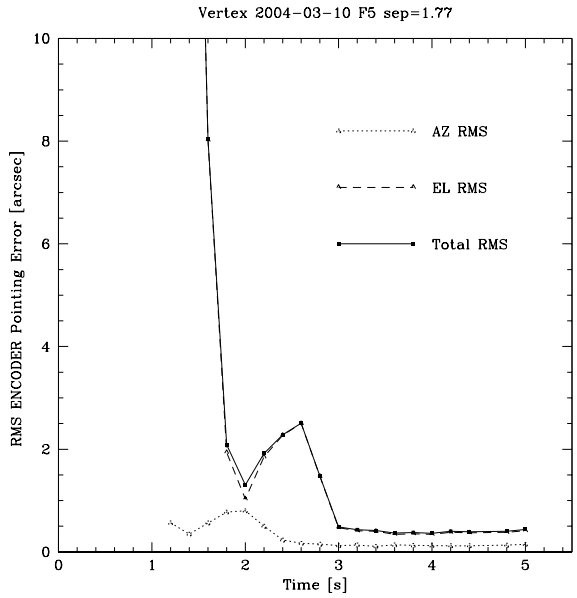

Figure 5.8: VertexRSI RMS encoder pointing error as a function of time since the start of a fast switching slew of 1.77 deg. The antenna takes about 1.8 s to get on source, and it does so with a 2 arcsec RMS pointing error, which decays to less than 0.5 arcsec at about 3 s.

5.3.2 Accelerometer Measurements

The fast switching performance investigation using the accelerometers is limited by the bandwidth of the equipment. For timescales longer than a few seconds, the low frequency cut-off of the equipment results in less accurate absolute values for displacements which follow a large acceleration. To aid in interpreting the results, encoder read–out has been taken into account as well.

During fast switching, the VertexRSI antenna experiences significant overshoots in azimuth and elevation pointing, which take some time to be corrected. Settling time to within 3 arcsec depends on the azimuth, elevation, and switching direction. For some directions, settling time is approximately 1.5 seconds, while for other conditions, an additional second may be needed to reach 3 arcsec pointing accuracy. After approximately 2.5 seconds, pointing has stabilised to a level which does not differ significantly from the RMS pointing stability, which is approximately 0.4 arcsec. The VertexRSI apex structure exhibits a negligible amount of rotation about its boresight axis and is not likely to contribute significantly to radio pointing errors.

5.4 On-The-Fly Performance

5.4.1 CANAlyzer Measurements

Measurements of the On-The-Fly (OTF) mapping performance of the VertexRSI antenna were made by comparing the commanded and actual encoder positions of the antenna

while executing a boustrophedonic[1] pattern on the sky. The OTF mapping performance is driven by the maximum velocity and acceleration performance of the antenna. There are two OTF mapping modes:

TPOTF: Total Power, or "single dish", OTF. The contract specification for this observing mode states that the antenna must:

1. Scan at a rate of up to 0.5 deg/s on the sky.
2. Turn-around as rapidly as possible, and scan back across the source in the opposite direction.
3. The source can be many beamwidths in size.
4. Precise antenna positioning is not necessary: it is sufficient to simply know where the antenna is actually pointing.

MOTF: Mosaic, or "interferometric", OTF. The contract specification for this observing mode states that the antenna must:

1. Scan at a rate of up to 0.05 deg/s on the sky.
2. Turn-around as rapidly as possible, and scan back across the source in the opposite direction.
3. The source can be many beamwidths in size.
4. The antenna must follow the commanded path to within 1 arcsec RMS pointing accuracy.

Software developed by Fritz Stauffer, called the "CANAlyzer", was used to gather the commanded and actual position information from the communications channel between the ALMA computer and the antenna computer (the CAN bus) in real-time as the antenna executed its OTF scan. A series of large OTF maps were made with varying row spacing and scan rate, representative of likely OTF map parameters. Figure 5.9 shows the position command and antenna response for both a TPOTF and MOTF scan velocity. Figure 5.10 shows the positioning errors measured for typical scan rows from a TPOTF and a MOTF mapping observation. Note that since the antenna is not required to follow a specified track during the TPOTF observations, the large cross-elevation errors measured do not violate the performance specification. For the MOTF scan row, the observing pattern was not optimized for these simulations. A small "ramp-up" and "ramp-down" region placed at the beginning and end of each row would allow the antenna to get on-track in cross-elevation, which would allow the antenna to meet the MOTF performance specification. In the example shown, the cross-elevation and elevation RMS become 0.83 arcsec and 0.45 arcsec, respectively, when four samples from each end of the scan are removed from the calculation.

[1]From the Greek "boustrophe-don": turning like oxen in plowing; from "bous": ox, cow; "strephein": to turn. An ancient method of writing using alternate left-to-right and right-to-left lines. It is also used for an optimisation performed by some computer typesetting software and moving–head printers to reduce physical movement of the print head. The adverbial form "boustrophedonically" is also found.

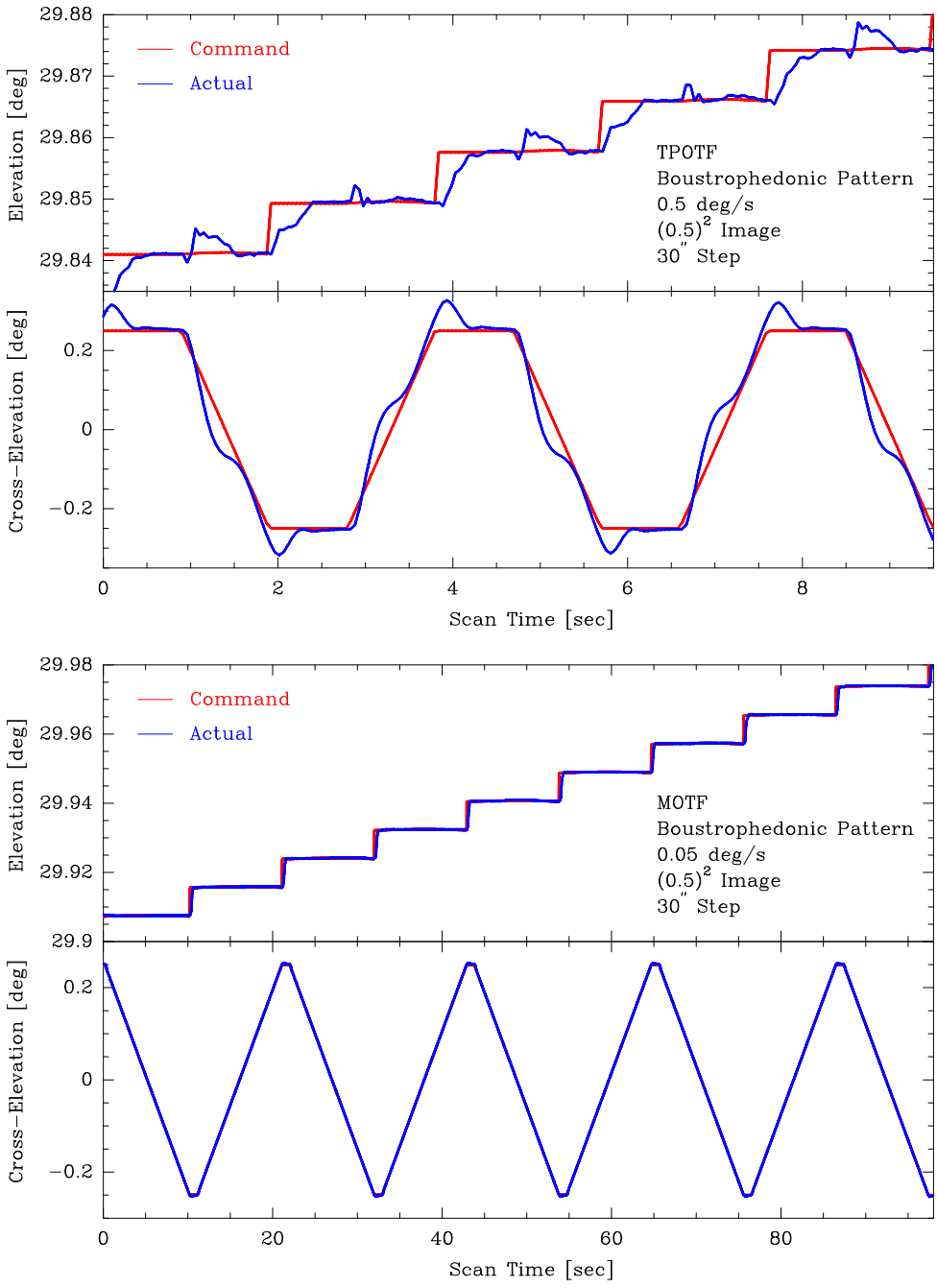

Figure 5.9: TPOTF (top) and MOTF (bottom) position command and antenna response for several scan rows. Between each row a 0.9 second turn-around time was included.

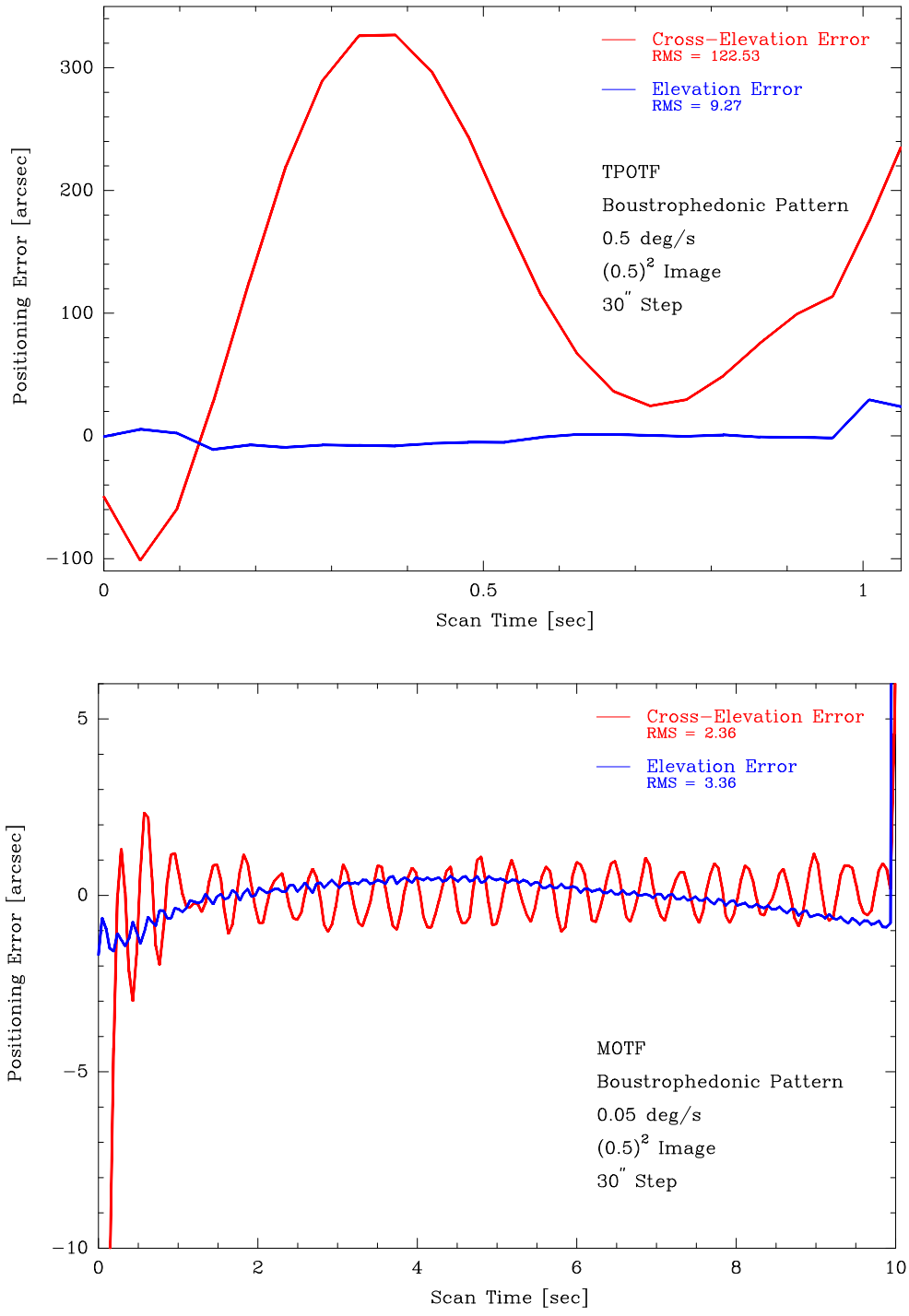

Figure 5.10: Positioning errors from typical scan rows from a TPOTF (top) and MOTF (bottom) mapping observation. Note that in the TPOTF observing mode the position of the antenna need only be known accurately. For the MOTF observation, a minor optimization in observing strategy, by adding a small "ramp-up" and "ramp-down" region placed at the beginning and end of each row would allow the antenna to get on-track.

5.4.2 Accelerometer Measurements

The accelerometers mounted at the rim of the BUS and encoders show somewhat different positions during the fastest angular accelerations for position slews. The effect amounts to approximately 2.1 arcsec for 1 deg/s^2 azimuth acceleration, and 2.8 arcsec for 1 deg/s^2 elevation acceleration. This will affect pointing accuracy during OTF patterns with high angular accelerations, *e.g.* where the scanning direction is reversed.

5.5 Path Length Performance

5.5.1 API Measurements

The path length performance was measured with a API Laser Interferometer to a precision of $\pm 1\mu$m. With this instrument it is *not* possible to measure the full path length variation between the receiver and the ground (foundation) with a single measurement, which would allow for the evaluation of the integrated behaviour of the antenna. The path length variations of several individual sections were measured instead, with the understanding that the full path length variation is approximately the sum (RSS) of the components. These measurements contain (see Figure 5.11):

L1: The path length between the ground (foundation) and the lower (stationary) part of the Az bearing; this path length variation concerns a steel section of the telescope;

L2: The path length of the (left) fork arm; this path length variation concerns a steel section of the telescope;

L3: The path length between the Invar ring and the apex of the subreflector; this path length variation concerns primarily the CFRP quadripod, but also the aluminum support of the subreflector (version of production telescopes without nutator).

L4: The path length between the apex (or receiver) and a point on the reflector surface. We did not succeed in measuring this path length variation.

The reported measurements cover the meteorological conditions of daily ambient air temperature changes up to 25 C, changes of the wind speed up to 15 m/s, and variable solar illumination.

The results are summarized in Table 5.1 as maximum variation (MAX) and minimum variation (MIN) during 24 hours of the day. Figure 5.12 shows the path length variations throughout the day during a 3 minute, 10 minute and 30 minute time interval. Although the path length measurements contain a significant systematic (and probably also predictable) component, in particular when considering time intervals around 1/2 hour (see Figure 5.12) and longer, so that statistical methods are no longer fully valid, the last row of Table 5.1 is obtained by RSS of the corresponding daily maximum path length variations. This is an upper limit to the actual path length variations, of which the values indicate that the path length specification is fulfilled.

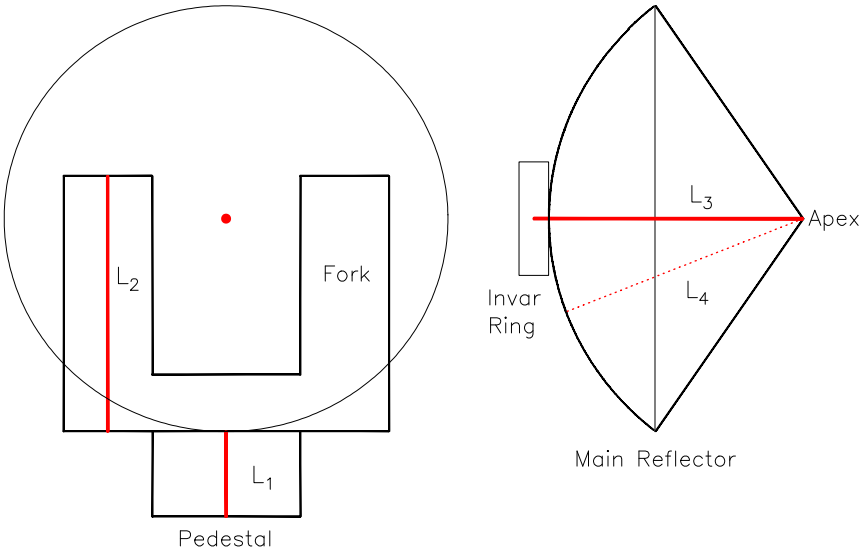

Figure 5.11: Schematic showing the path length sections which comprise a total path length variation measurement.

We find that the long–term path length variations of steel components (pedestal, fork arms) can be predicted from monitored temperatures, as illustrated in Figure 5.13 as a representative example. The daily path length variation of the pedestal and the fork arm is correlated with the variation of the steel temperature of these parts; the path lengths can be predicted from (simple) measurements of the steel temperature (2 to 3 sensors), either used in an empirical way, or used in a more refined way in a FEM; the calculated predictions based on the readings of the temperature sensors and the ANSYS model of the VertexRSI antenna agree with the measured path length variations.

The left–side panel of Figure 5.13 shows the average temperature (red dots) of the fork-arm derived from the 14 temperature sensors. The maximum and minimum temperature of the fork-arm is shown by the dashed lines. The right–side panel of Figure 5.13 shows the measured daily path length variation L2 (black line). The red dots represent the path length variation derived from the measured temperatures used in a FEM calculation. The measurement of the temperature at few locations in the fork-arms and application of the thermal dilation relation is adequate for a long-term prediction.

We conclude from these measurements that the path length stability meets the specification, under normal observing conditions as well as all motions of the telescope, in particular fast-switched motions. Within the path length specification, there exists a large systematic hourly and daily component to the path length variations of the steel components of the telescope which is due to thermal effects and which can be predicted with good accuracy from temperature measurements.

5.5.2 Accelerometer Measurements

Path length jitter on timescales of several seconds was determined from the BUS boresight motion with respect to ground, and the differential boresight motion of the subreflector

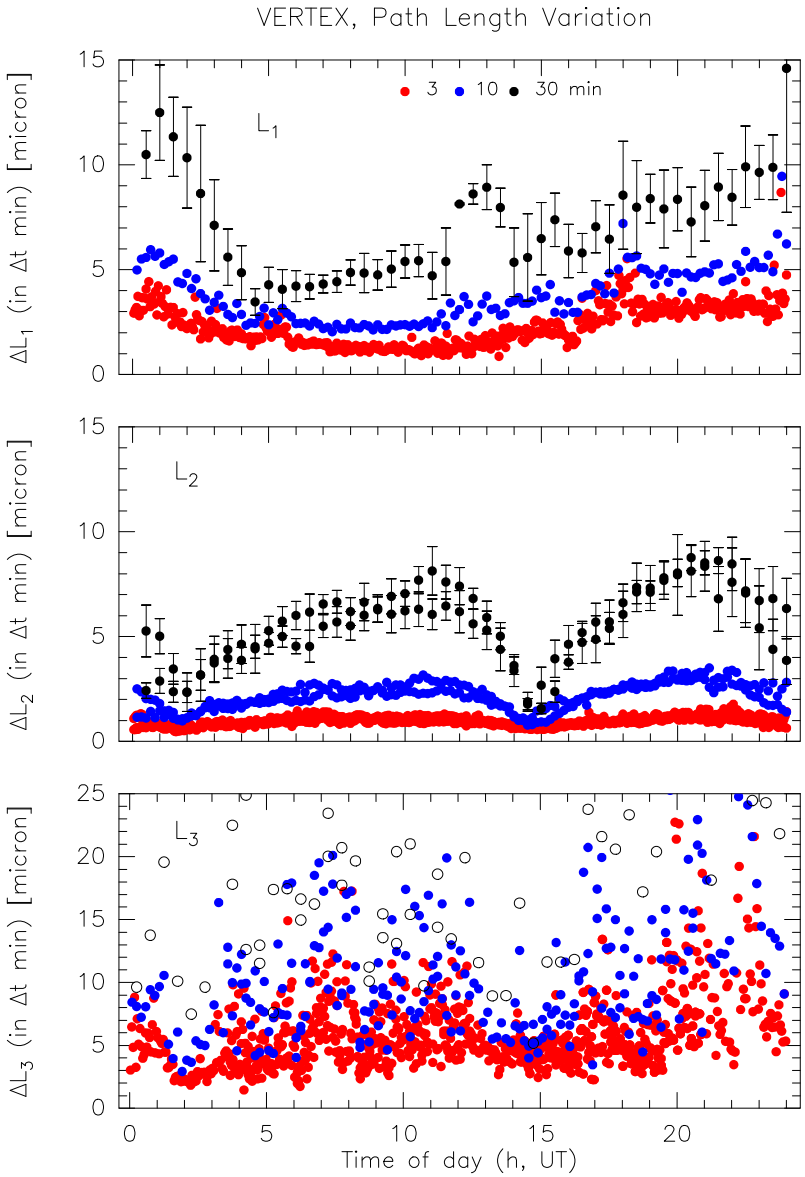

Figure 5.12: Variation of path length L1: pedestal, of path length L2: fork arm, and of path length L3: Invar ring to subreflector, as a function of the time of the day (UT), and within intervals of 3 minutes (red), 10 minutes (blue), and 30 minutes (black) duration. Note the difference in scale. The error bars are RMS values for a 30 minute time interval. For the displayed values ΔL3, the thermal dilation of the aluminum subreflector support and the support of the API has been eliminated. Local time = UT $-$ 6 hours.

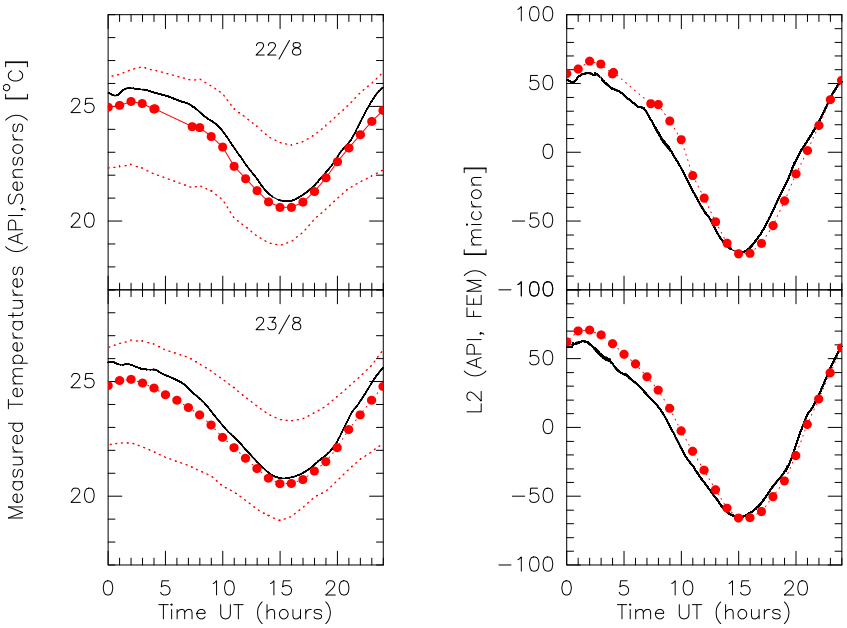

Figure 5.13: Predictability of the long–term path length variation of the steel components from temperature measurements on the VertexRSI antenna, illustrated for the left fork arm on 2003/08/22 and 2003/08/23. Left–side: temperature measurements at the API instrument: black line; average temperature of the fork arm derived from temperature sensors: red dots; maximum and minimum temperature of fork arm: dashed lines. Right–side: API measured path length variation: black line; path length variation predicted from the corresponding temperature measurements (left–side) used in the FEM: red dots.

Table 5.1: VertexRSI Prototype Antenna Path Length Variations

Path Length	3 min		10 min		30 min		$t_{measure}$
	MIN (μm)	MAX (μm)	MIN (μm)	MAX (μm)	MIN (μm)	MAX (μm)	(hours)
L1: pedestal	1.5±0.5	3±1.0	2±1.0	6±2.0	4±2.0	10±3.5	250
L2: fork-arm	0.5±0.25	1.5±0.5	1±0.5	3±1.0	3±1.0	8±2.0	360
L3: feedleg[a]	3	5	3	5	5		25
L4: reflector[b]	∼5		∼7		∼9		est.
Total Path Variation[c]	≤8		≤10		≤15		...

[a]L3: The values of the thermal influence of the aluminum subreflector and API are removed.
[b]L4: Estimated value (approximated from CFRP behaviour of BUS and quadripod).
[c]RSS of the corresponding daily maximum path length variations, which represents an upper limit to the actual path length variations.

with respect to the BUS. For sidereal tracking and wind effects, path length stability is typically within a few microns over these timescales.

5.6 Focus Performance

We have several independent measurements of the change in focal length of the primary reflector of the VertexRSI antenna as functions of elevation angle and ambient temperature.

5.6.1 Elevation Dependence

Multiple measurements and calculations of the focus performance of the antenna have been performed:

1. The photogrammetric surface measurements of the VertexRSI antenna were performed at 5 different elevation angles. From these data the focal length of the best fit paraboloid has been calculated.

2. With the quadrant detectors and API system we have measured the deformation of the reflector edge and the change in subreflector position. These data provide the change in focal length as well as the lateral displacement of the subreflector.

3. VertexRSI has provided us with the FEM calculated change in focal length of the main reflector and the axial and lateral shift of the subreflector.

4. The radiometric measurements also deliver data on the change in focus. In this case, the measurements reflect the change as a result of both a variation of elevation angle

and in ambient temperature. The data have been analysed to yield the change in focus position as function of these two variables individually. The following expression represents the change in axial focus position:

$$\mathrm{Z-focus(mm)} = 1.858\sin(El) + 0.036T(C) - 0.034.$$

The results of the measurements are summarised in Figure 5.14. There is a good agreement between the values measured using different methods. The difference between the FEM and the measurements suggests that the BUS is slightly less stiff and the quadripod more stiff than that predicted by the FEM.

5.6.2 Temperature Dependence

From the radiometer and holography measurements we have derived the change in best-fit focal length of the primary reflector as a function of temperature. From holography maps, spanning an ambient temperature from 11 to 33 C, the focal length indicates a linear change of 34 μm/C. As shown in the formula above, the radiometer measurements show a change of 36μm/C over a temperature range of -8 to 24 C. The agreement between these two determinations is remarkable. All measurements with a linear fit are shown in Figure 5.15.

The specification states that a refocusing will be done every 30 minutes, whereby it is assumed that the ambient temperature will change by not more than 1.8 K/30 min. Thus a focus change, and hence a path length variation of 100μm (twice the focus change) between two focus calibrations can occur. This is a highly repeatable error which will be almost the same for all antennas in the array. By measuring the temperature it can be quite accurately corrected, if desired.

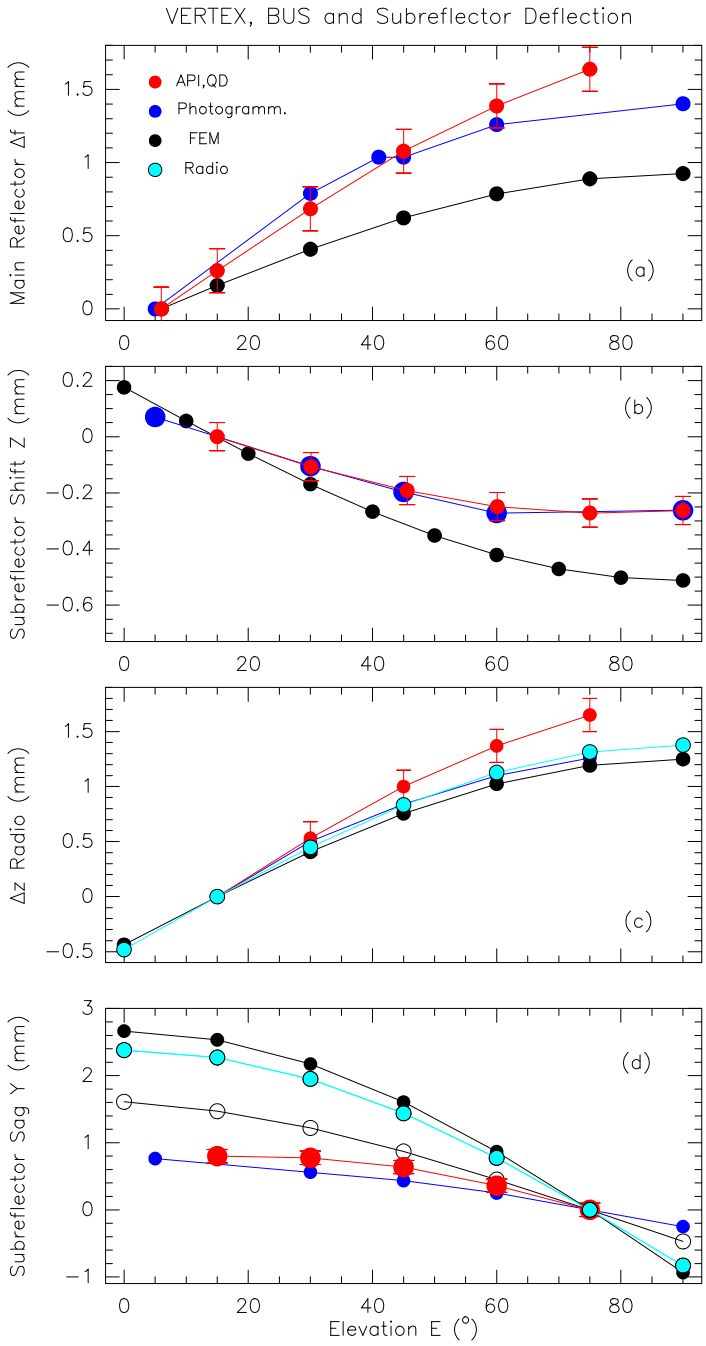

Figure 5.14: Mechanical (API,QD, Photogrammetry) and radio measurements of the BUS deflection and subreflector (quadripod) deflection, as a function elevation, and compared to FEM calculations. (a) Change in focal length of the main reflector; (b) Change of distance between the Invar ring and the subreflector apex; (c) focus change determined from radio observations, the red curve is the focus change predicted from the mechanical measurements shown in (a,b); (d) sag of the subreflector in vertical direction (sag Y): the black dots represent the prediction of the FEM calculation as to be used for the radio observations, the open circles represent the FEM prediction to be compared with the mechanical measurements, the light blue dots the radiometrically required Y translation of the subreflector.

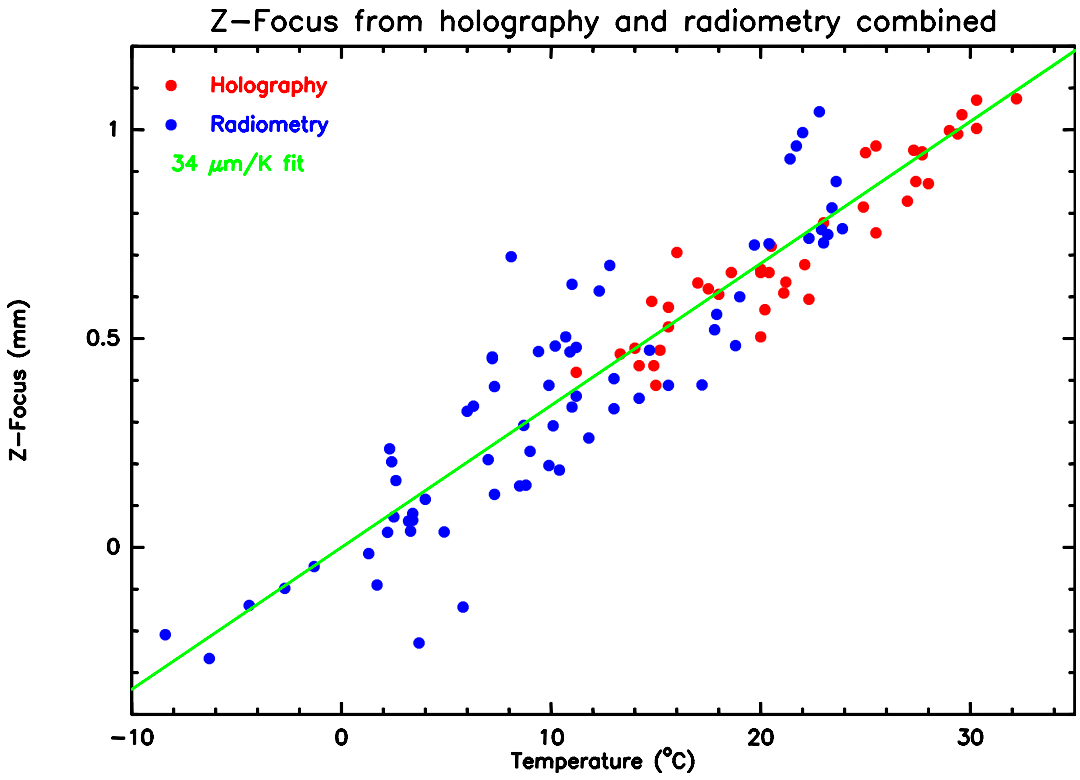

Figure 5.15: The change in focal length as a function of the ambient temperature derived from radiometer and holography measurements. The good linear fit gives 34μm/C change.

Chapter 6

Evaluation Results for the AEC Prototype Antenna

6.1 Surface Accuracy Performance

6.1.1 Holography

The specification requires the antenna to have a surface accuracy of 25μm RMS with a goal of 20μm. The initial surface setting was performed by AEC with a Leica laser-tracker to 50μm RMS. Equipment and methodology for the holographic measurements were identical to those used on the VertexRSI antenna (see §5.1.1).

The first holographic measurements of the AEC antenna indicated that the position of the feed in the nominal "mechanical" primary focus was displaced from the focus of the best–fit paraboloid by ~ -5mm in Y and $\sim +12$mm in Z. As the positioning of the holography signal feed was not nearly as stable as it was on the VertexRSI antenna, we felt that the contractor–determined focus of the reflector was more reliable. Hence, no refocus setting of the AEC antenna surface was made. This has been confirmed by recent measurements of the apex location by the contractor who determined displacements of -9mm in Y and $+8$mm in Z.

We reached a surface RMS of 15μm after two complete and one partial adjustment. Also in this case we made numerous surface maps over several days to study any influence of the changing environmental conditions. None could be found with any significance. In Figure 6.1 the time sequence of a series of measurements is shown, indicating the high stability of the surface over time. The hardware lay-out of the receiver was slightly different in this case and no artifacts were seen in the data.

The adjustments were done with a tool provided by the contractor, similar to the one used by us on the VertexRSI antenna. The time needed for an adjustment of the total of 600 adjusters was 6.5 hours, easily meeting the specification of maximally 8 hours.

6.1.2 Radiometric Beam Maps

At the relatively long wavelengths available ($>$ 3mm during the observing period made available to us) it is not really feasible to characterize the antenna surface by means of

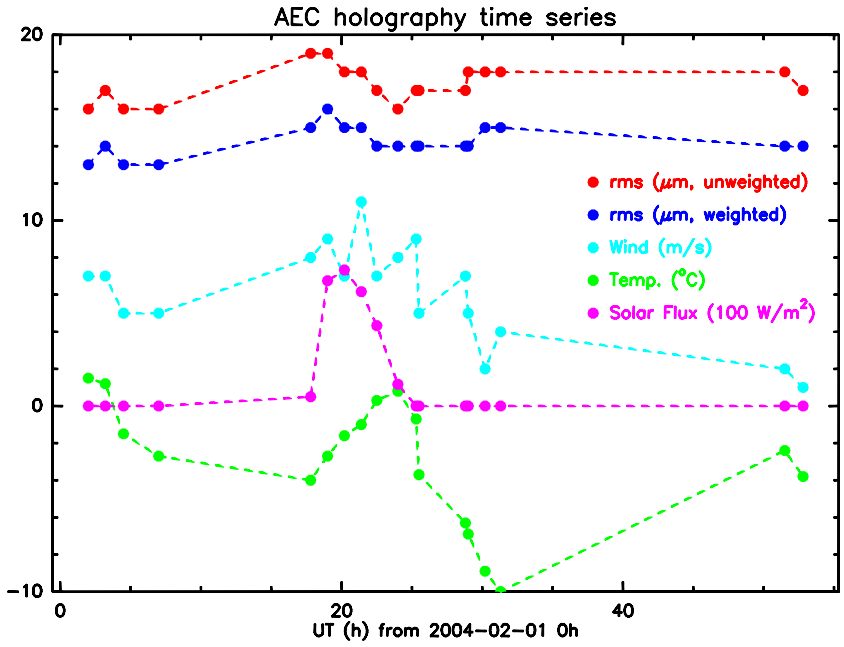

Figure 6.1: Time series of the holography of the AEC antenna over a period of three days in February 2004. The weighted (applying the illumination function, taper) and unweighted RMS values are given along with temperature, wind speed and solar flux. There is no discernible influence of the varying environmental parameters on the RMS values.

beam shape measurements. We have, though, been able to make clean maps of Mercury (Figure 6.2).

6.2 Pointing Performance

6.2.1 Optical Telescope and Radiometric Measurements

1. All-Sky Pointing

   (a) All–sky OPT data for the AEC antenna are available for the period from 2004 March 6. As for the VertexRSI antenna, it was possible to identify a pointing model that consisted of a fixed core of ten semi-empirical but mechanically plausible harmonic terms plus the expected five zero-point, boresight and tilt terms. Within the fixed core, the vertical deflection was pure Hooke's-Law, and the highest frequency terms were 6×azimuth.

   (b) Plots of cross–elevation (horizontal) residuals against azimuth revealed noise of an abnormal and quasi–periodic character, with especially poor performance in the NNE and SSW. After applying the adopted 15–term model, quasi–periodic effects remain visible; they can be beaten down by adding extra empirical terms, but without a significant reduction in overall sky RMS. Cross–elevation residuals increased at higher elevations, proving that the noise is not simply in the

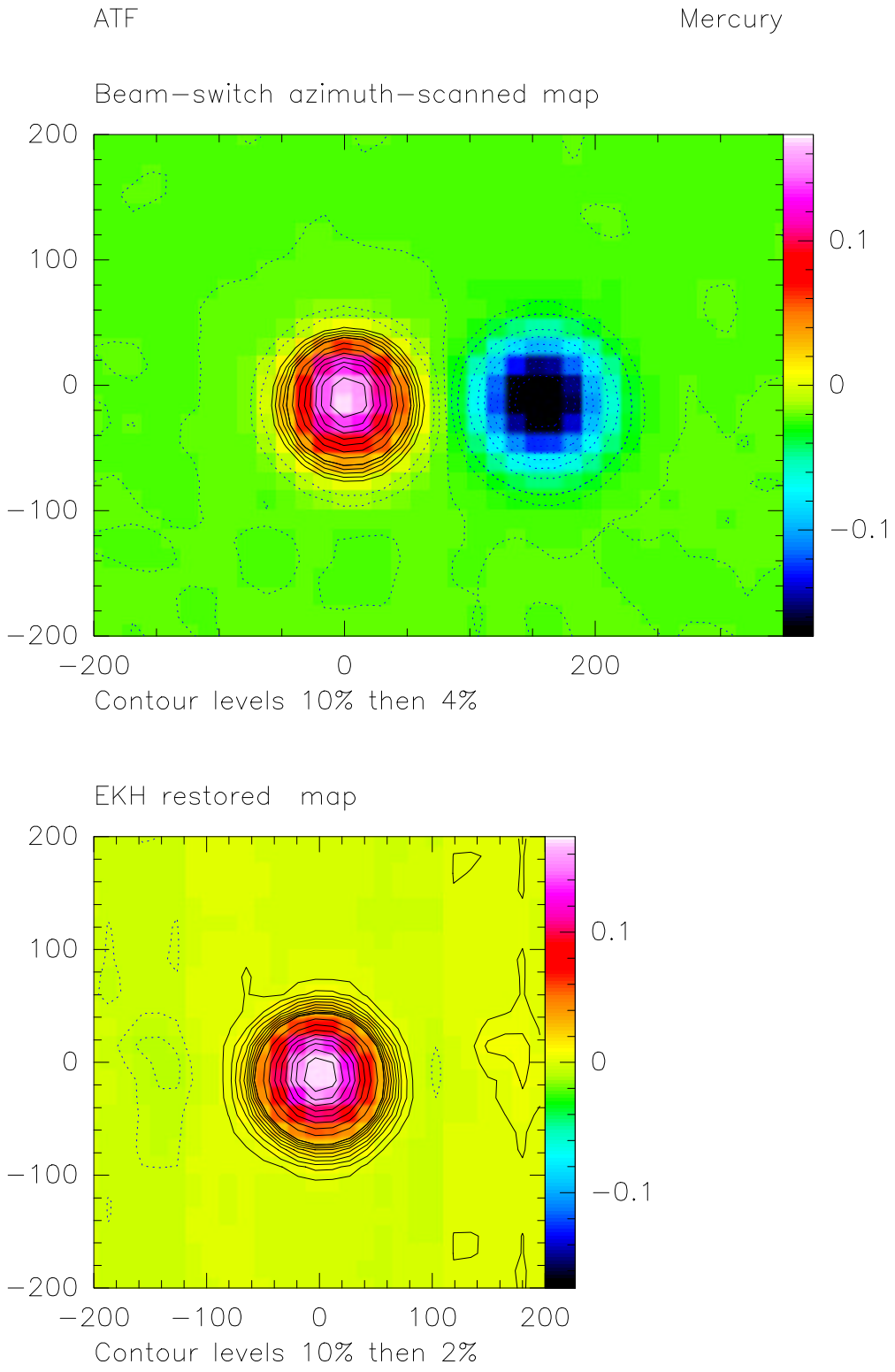

Figure 6.2: Planet Mercury observed at 95 GHz with the AEC antenna: angular distance from the Sun was 25 degrees; the planet angular diameter was 7.2″; contour levels are $4, 8, 12, 16, 20, 30, ...90\%$. Top: raw beam–switched map (beam separation 160″); bottom: map restored with the EKH algorithm; contour levels are $2, 4, 8, ..., 16, 18, 20, 30, ...90\%$

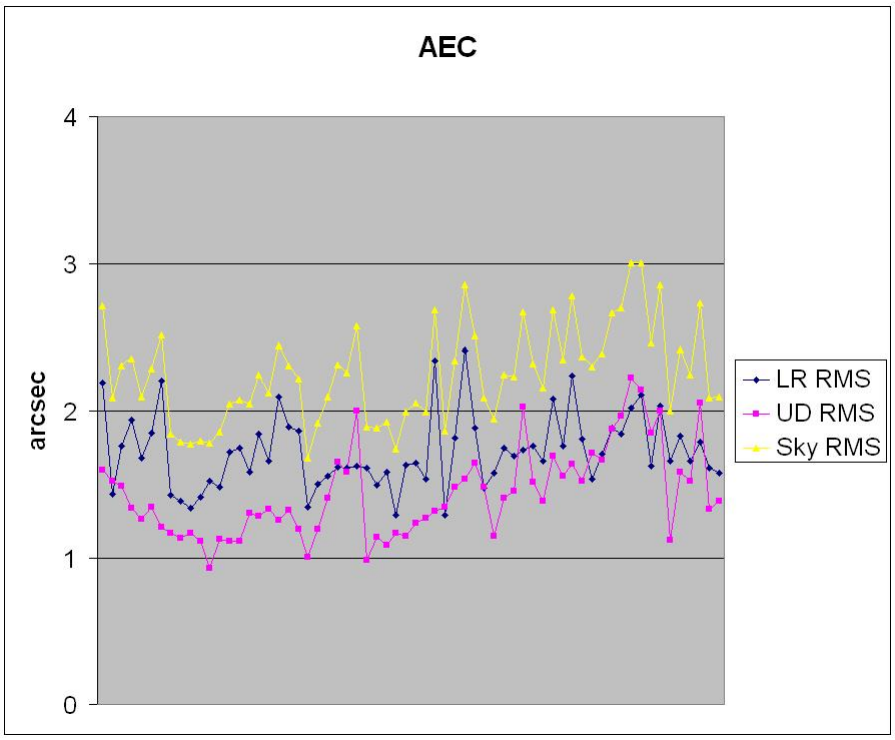

Figure 6.3: The all–sky optical pointing performance of the AEC prototype antenna. The cross–elevation performance (the line labeled "LR RMS") is noticeably worse than the elevation performance ("UD RMS"). The elevation performance is similar to that found on the VertexRSI prototype antenna and may be local optical seeing effects. The poorer cross–elevation performance is thought to be evidence of instability in the azimuth bearing. Although some tests reach the 2 arcsec all–sky specification, most fall somewhat short.

azimuth readings. Instability in the azimuth bearing seems to be the best explanation, causing changes in both elevation and Az/El non-perpendicularity.

(c) In a total of 64 runs spanning about two months, the sky RMS was between 2 and 2.5 arcsec (see Figure 6.3). The scatter was usually about 50% larger in the horizontal direction than in elevation. The scatter in elevation is comparable to that from the VertexRSI prototype antenna (averaging 1.43 arcsec in the AEC case versus 1.36 arcsec in the VertexRSI case) and exhibits similar slow variations. This suggests that the elevation performance of both prototype antennas is significantly affected by local weather and/or seeing effects, and demonstrates how the AEC all–sky RMS is dominated by the poor cross–elevation performance.

(d) The pointing model was satisfactorily stable. The zero-point and boresight terms IA, IE and CA, were constant to ±3 arcsec except for occasions when mechanical adjustments had been made or metrology arrangements changed. The tilt terms, AN and AW, varied by about ±1 arcsec. The prospects for keeping the pointing tuned by 5-star recalibration runs once or twice a day seem very good.

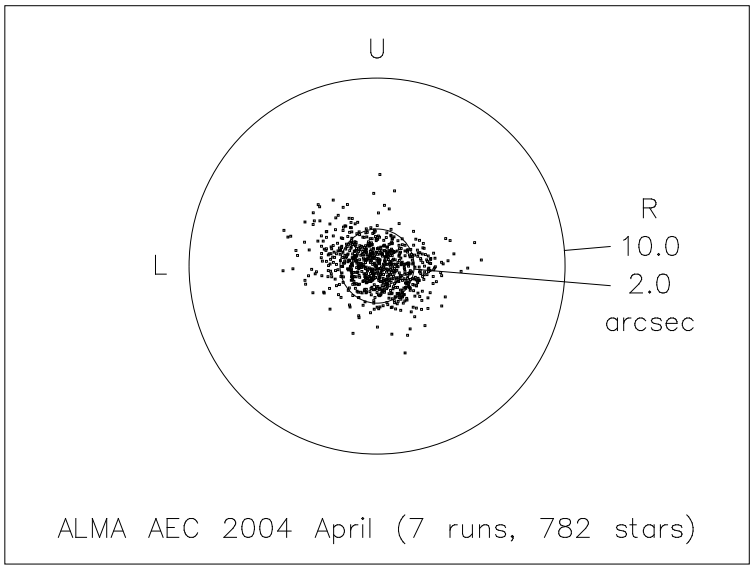

Figure 6.4: A particularly good all-sky optical pointing result for the AEC prototype antenna. The 782 observations span 8 hours and have simply been concatenated. The only adjustment that has been applied to the raw data is the removal of small drifts totaling about 2.6 arcsec horizontally and 1.9 arcsec vertically. The pointing model consists of a fixed core of ten simple correction terms, that applies to all the AEC OPT runs, with a further five terms (encoder and boresight offsets plus mount tilt) that are fitted to each individual run.

(e) The scatter diagram in Figure 6.4 is an example of the best all-sky pointing performance that the AEC antenna has given to date. The scale is the same as for the comparable VertexRSI plot (Figure 5.3).

(f) The radio tests are too few and limited in sensitivity to measure the actual all–sky pointing accuracy. Four runs, on separate days spanning about a week, totaling 155 radio sources, each delivered a pointing RMS in the 3–4 arcsec range. Hints of cross–elevation drifts were seen in one run, which if real would represent a cross–elevation pointing drift of less than 1 arcsec/hour.

(g) As mentioned previously, one aspect of the all–sky pointing specification calls for a recalibration of the pointing model only once a month. To investigate this in the case of the AEC prototype antenna, we selected two good OPT all–sky data sets taken about a month apart. The first data set was used to fit the AEC standard model, with the fixed core left at the nominal values. The Sky RMS of this "operational model" was 1.80 arcsec (*n.b.* most AEC all-sky tests are not this good). The second data set was fitted to the operational model, with only the boresight terms IE and CA allowed to vary. This adjusted model gave a sky RMS of 2.38 arcsec. If, in addition to the IE and CA terms, the tilt terms AN and AW are allowed to vary, the sky RMS is a slightly better 2.2 arcsec. The improvement gained from fitting all four terms is modest. A further significant gain, to 2.0 arcsec RMS, was achieved by allowing the Az/El non-perpendicularity term, NPAE, to vary in addition to the previous four. In

fact the change in the NPAE coefficient, +3.4 arcsec, was larger than any of the others: This variable non-perpendicularity is thought to be caused by problems in the azimuth bearing, and contrasts with the comparative stability of the rest of the model.

2. Offset Pointing

   (a) The offsetting performance was sampled by using the OPT to observe a small number of stars in a small area of sky repeatedly. With the standard pointing model engaged, including recent estimates of IA, AN and AW, only the overall boresight offsets IE and CA were fitted. In a four–star field that was tracked from 20° to 8° zenith distance, two of the stars were systematically displaced from the mean by just over 0.6 arcsec, marginally greater than the specification. However, it seems clear that this level of offset pointing accuracy is simply another aspect of the all–sky performance and the suspected instability in the azimuth bearing.

   (b) The radiometric determination of relative pointing accuracy can be limited by atmospheric seeing, though at a lower level than for optical determination. From repeated measurements of Jupiter in good atmospheric contitions, we obtained an upper limit of ~ 0.4 arcsec to the pointing measurement repeatability. Experiments where we switched between the halfpower point on Jupiter and a position 1.5 degrees away show very small radiometrically determined position errors, and are limited by a 5 Hz oscillation at a level of 0.4 arcsec peak to peak when the antenna is settled (after 2.0 seconds).

   (c) Experiments where we continuously tracked the half-power points of Jupiter under low-wind conditions over time intervals of a 10–30 minutes show encoder errors at the level of 0.03 arcsec RMS on both axes (.041 arcsec total). The radiometrically measured pointing errors are quite a bit larger, at the 0.6 arcsec level and are of atmospheric origin (the radiometer noise contributes only to 0.2 arcsec RMS).

6.2.2 Accelerometer Measurements

For sidereal tracking under *low wind conditions*, the RMS all sky BUS pointing jitter over periods of 4 seconds is 0.054 ± 0.048 arcsec for the AEC antenna.

Wind performance as measured at the ATF (780 mbar pressure), scaled to 9 m/s average wind and 560 mbar pressure, following the weighting table in the Statement of Work, amounts to 0.22 ± 0.11 arcsec RMS over timescales of 4 seconds. This number excludes the effects of sidereal tracking.

The combined wind and sidereal tracking performance at timescales of 4 seconds, taking into account the pressure difference between the ATF and Chajnantor, amounts to 0.23 ± 0.12 arcsec. Figure 6.5 shows the BUS RMS pointing stability for the AEC antenna for 9 m/s wind at Chajnantor pressure.

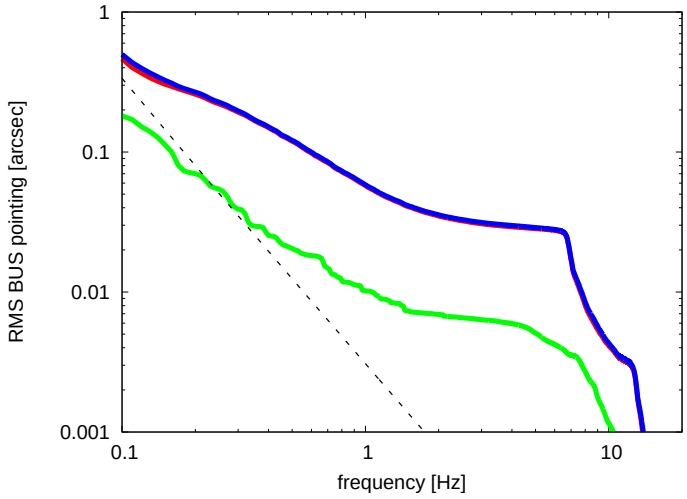

Figure 6.5: RMS BUS pointing and tracking stability for the AEC antenna for 9 m/s wind at Chajnantor pressure. The red curve shows the effect of wind, without the effect of sidereal tracking. The green curve shows the effects of sidereal tracking for low wind conditions. The blue curve shows the combined effect of wind and sidereal tracking. The dashed line is an estimate of the noise in the blue curve. Each point in the curve shows the RMS pointing for that frequency and above, or alternatively over time periods corresponding to the frequency.

6.3 Fast Switching Performance

6.3.1 Optical Telescope and Radiometric Measurements

We have studied the fast switching performance of the AEC prototype antenna using analyses of encoder, optical telescope, and radiometric measurements. Just as for the VertexRSI prototype, we see very similar results in all of the slewing profiles for this antenna.

The radiometric data for the AEC antenna was collected and processed as indicated for the Vertex antenna, but the individual slewing scans were 10 s rather than 5 s. Rather than make the plots on the same time scale, we reproduce the entire slew scan length. The mean radiometrically–inferred and mean encoder pointing errors as a function of time since the start of the 1.5 deg fast switching slew are illustrated in Figure 6.6. The source is reached with 3 arcsec accuracy about 1.5 s after the start of the slew, about 1 arcsec after 1.8 s, and under 0.2 arcsec RMS after 2 s. A 5 Hz mechanical pointing oscillation is excited by fast switching antenna motions, but this oscilation has a peak to peak amplitude of 0.4 arcsec or less, damps out in a few seconds, and is not seen in tracking data (only when the antenna is abruptly started and stopped as in fast switching). The 1-2 s period pointing "waves" in the slewing profile are due to atmospheric pointing fluctuations, and after settling, the mechanical pointing is very small (less than 0.1 arcsec RMS).

Figure 6.7 shows a typical optical fast switching measurement. The antenna takes just 1.6 seconds to get from one source to another source 1.76 degrees away with 1 arcsec pointing errors. (Note that the 3 arcsec pointing error specification is met in just under

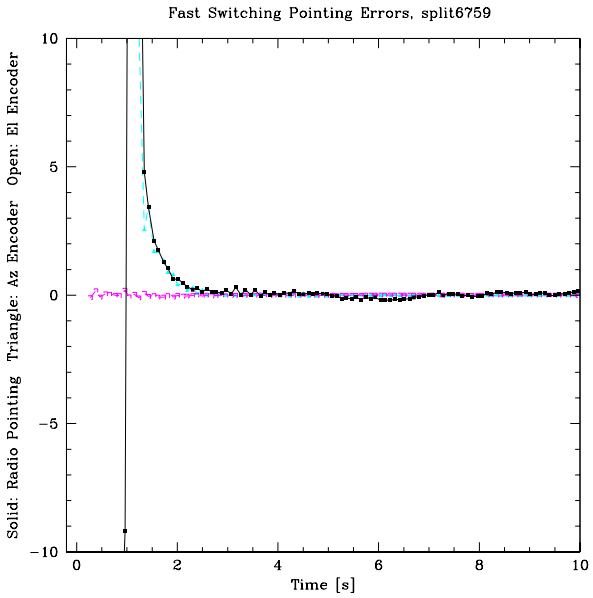

Figure 6.6: Radiometric fast switching measurement for the AEC antenna. The mean radiometrically-inferred and mean encoder pointing errors as a function of time since the start of the 1.5 deg fast switching slew are shown. The source is reached with an accuracy of 3 arcsec pointing error about 1.5 s after the start of the slew, 1 arcsec after 1.8 s, and after 2 s, the RMS pointing error is under 0.2 arcsec.

1.4 s). The pointing errors are flat and essentially atmosphere limited beyond 1.6 s.

Figure 6.8 shows RMS encoder pointing errors for the same series of fast switching slews between the two sources 1.76 deg apart. There seems to be a latency issue with the optical data, as the two curves are shifted by almost 0.2 s, with the encoders showing up earlier than the optical pointing. The encoders indicate the AEC antenna gets on source with the 3 arcsec fast switching pointing specification between 1.3 and 1.4 s, and has RMS pointing errors of under 0.5 arcsec for 1.6 s after the start of the slew. The fast switching slew is very clean, and the servo system seems to be very well-tuned to this sort of antenna motion.

6.3.2 Accelerometer Measurements

The fast switching performance investigation using the accelerometers is limited by the bandwidth of the equipment. For timescales longer than a few seconds, the low frequency cut-off of the equipment results in less accurate absolute values for displacements which follow a large acceleration. To aid in interpreting the results, encoder read–out has been taken into account as well.

During fast switching, the AEC antenna experiences no visible overshoots in azimuth and elevation pointing, with the exception of some sub–arcsecond resonances, mostly in elevation, which damp out after a few seconds. Settling time to within 3 arcsec is under 1.5 seconds, for small pointing offsets. After approximately 3 seconds, BUS pointing has stabilised to a level which does not differ significantly from the RMS BUS pointing stability,

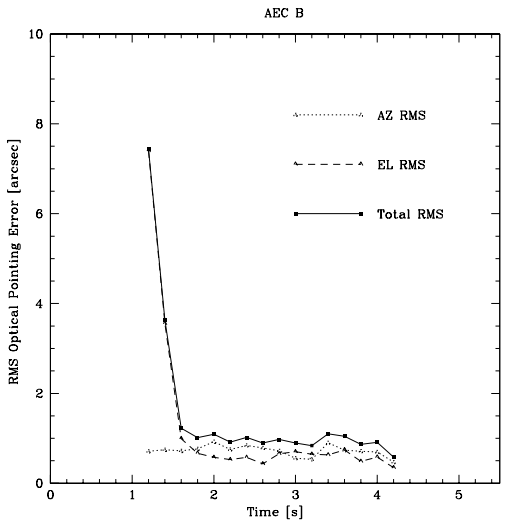

Figure 6.7: Example measurement of the RMS optical pointing offset as a function of time for the AEC antenna. The mean pointing offset during the last half of each 4 s fast switching slew and settle cycle has been subtracted, and the RMS optical pointing is then calculated for all measurements that fall in a given time bin. A total of 9 minutes, or 136 slewing cycles, were used to generate this plot. Embedded in these RMS pointing values are the results of the dry atmospheric fluctuations, or optical seeing, so the mechanical RMS pointing errors should be less than these values.

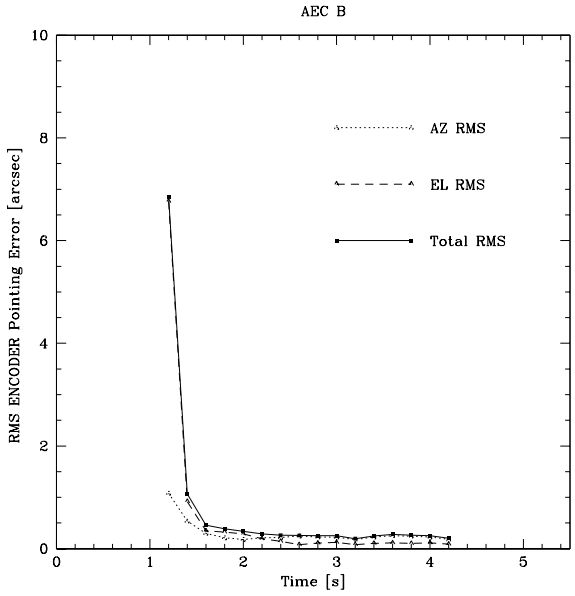

Figure 6.8: Fast switching measurements for the AEC antenna. The raw RMS encoder pointing errors for a series of fast switching slews between two sources 1.76 deg apart are shown. The AEC antenna gets on source with the 3 arcsec fast switching pointing specification between 1.3 and 1.4 s, and has RMS pointing errors of under 0.5 arcsec for 1.6 s after the start of the slew.

which is below 0.1 arcsec.

The apex structure rotates about an axis which is assumed to be aligned with the boresight axis, but offset by -1.5 to $+1$ cm depending on the elevation. Fast switching can excite the rotation mode, which has translation components on–axis which can amount to 30μm peak–to–peak. The rotation and corresponding translation component is at 5 Hz, and damps out with a $\frac{1}{e}$ decay time of 5 seconds. With the prime focus plate scale of 34 arcsec/mm, this translates to radio pointing errors of up to 1 arcsec peak–to–peak in cross-elevation, provided that the rotation axis is parallel to the boresight axis.

6.4 On-The-Fly Performance

6.4.1 CANAlyzer Measurements

Measurements of the On-The-Fly (OTF) mapping performance of the AEC antenna were made by comparing the commanded and actual encoder positions of the antenna while executing a boustrophedonic pattern on the sky. See §5.4.1 for descriptions of the two types of OTF mapping modes.

Using the "CANAlyzer" system described in §5.4.1, a series of large OTF maps were made with varying row spacing and scan rate, representative of likely OTF map parameters. Figure 6.9 shows the position command and antenna response for both a TPOTF and MOTF series of scans. Note the extreme overshoots in azimuth during irregular scan intervals. Figure 6.10 shows the positioning errors measured for typical scan rows from a TPOTF and a MOTF mapping observation. For the MOTF observing mode, the antenna performed remarkably well.

6.4.2 Accelerometer Measurements

The accelerometers mounted at the rim of the BUS and encoders show somewhat different positions during the fastest angular accelerations for position slews. The effect amounts to approximately 1.6 arcsec for 1 deg/s^2 azimuth acceleration, and 2.1 arcsec for 1 deg/s^2 elevation acceleration. This will affect pointing accuracy during OTF patterns with high angular accelerations, *e.g.* where the scanning direction is reversed.

6.5 Path Length Performance

6.5.1 API Measurements

As illustrated in Figure 5.12, the objective of the investigation was the measurement of the path lengths L1, L2, L3 and L4, for a representative period of time and a variety of environmental conditions. This objective is only partially achieved. The structure of the AEC antenna does not allow the measurement of the path length L1 (pedestal), in particular when the antenna moves. For L3, the measurement was only taken during a short period of time; the measurement of L4 was not tried because of late delivery of the antenna.

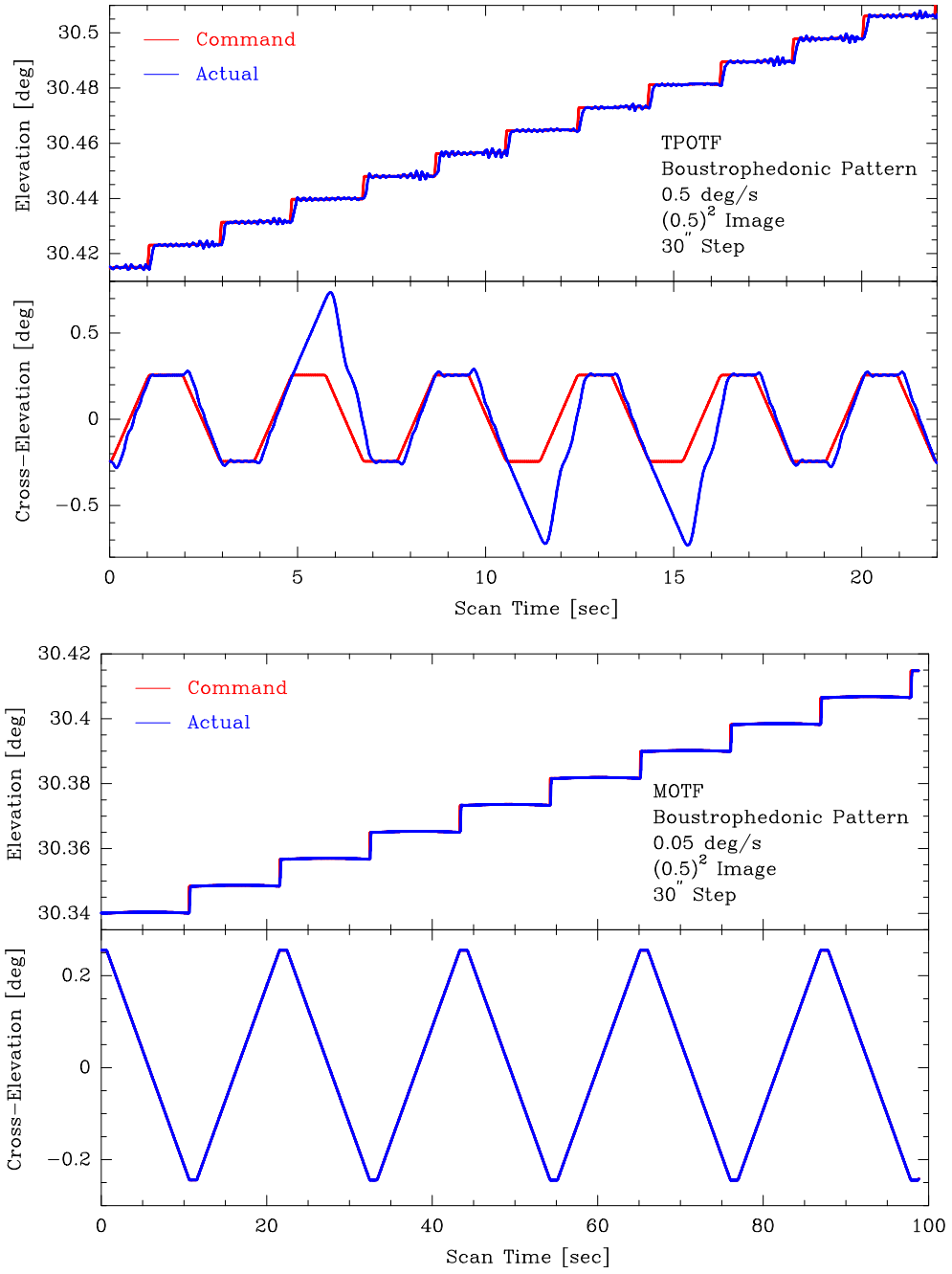

Figure 6.9: TPOTF (top) and MOTF (bottom) position command and antenna response for several scan rows. Between each row a 0.9 second turn-around time was included.

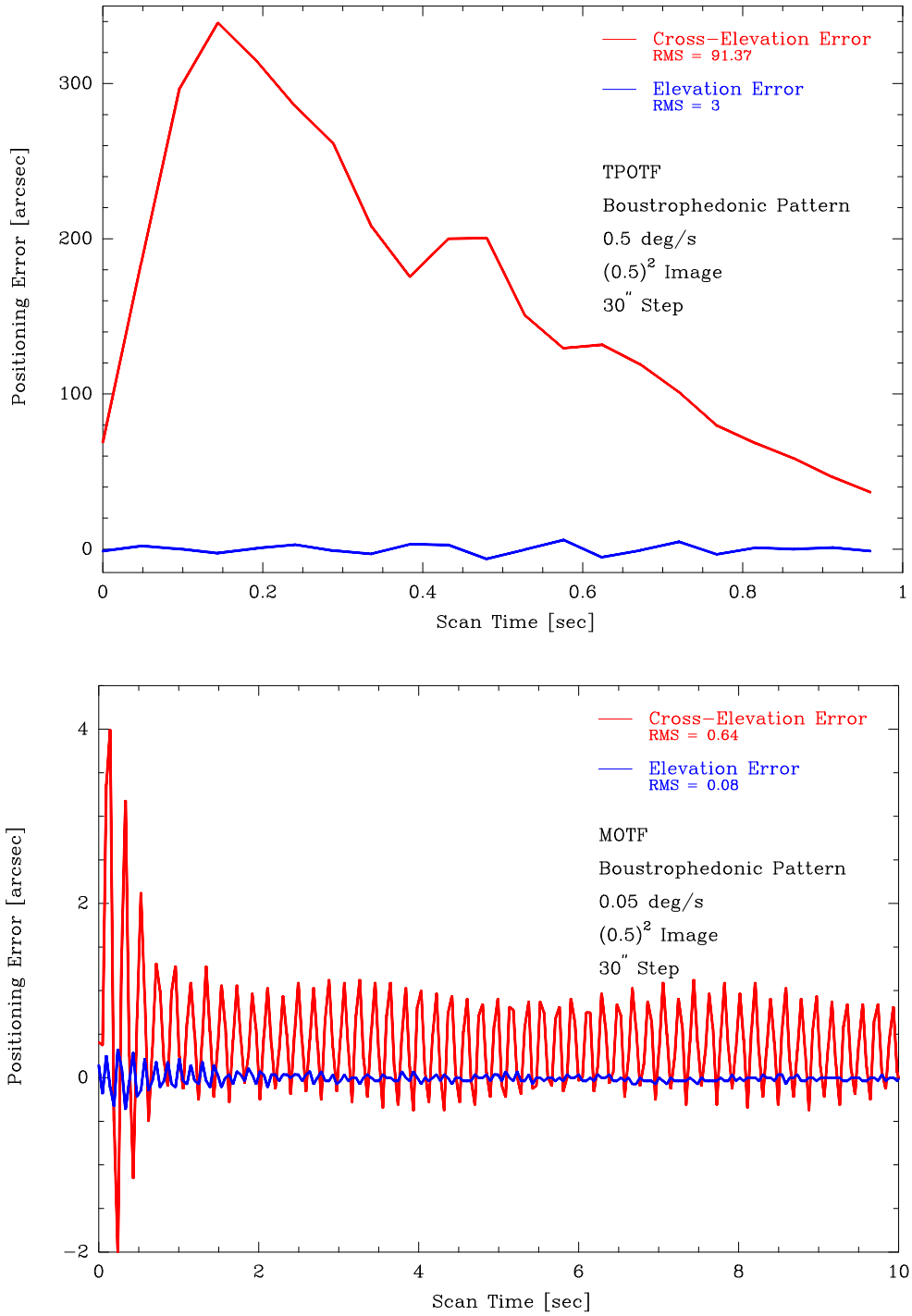

Figure 6.10: Positioning errors from typical scan rows from a TPOTF (top) and MOTF (bottom) mapping observation. Note the excellent performance for the MOTF observation. Two features in the MOTF plot are of note: (1) The $\sim$ 0.5 arcsec offset between the commanded and actual cross–elevation position is due to software error in the command response from the AEC ACU. Other measurements indicate that the antenna tracks the commanded position properly. (2) The cross–elevation position oscillation is due to feedback of the 5 Hz apex jitter into the cross–elevation servo.

Table 6.1: AEC Prototype Antenna Path Length Variations

Path Length	3 min (μm)	10 min (μm)	30 min (μm)	t_{meas} (hours)
L1: pedestal[a]	$\sim$5	$\sim$5	$\sim$5	est.
L2: fork arm	1–3	2–4	10$\pm$4	360
L3: feedleg[b]	4	5	$\sim$10	25
L4: reflector	$\sim$5	$\sim$5	$\sim$5	est.
Total Path Variation[c]	$\leq$10	$\leq$10	$\leq$25	...

[a]L1: Estimated value.

[b]The values of the thermal influence of the subreflector support (nutator, steel) and the API support are removed.

[c]RSS of the corresponding daily maximum path length variations, which represents an upper limit to the actual path length variations.

The result of the path length measurements is summarized in Table 6.1 and Figure 6.11. Although the path length measurements contain a significant systematic (and probably also predictable) component, in particular when considering time intervals around 1/2 hour (see Figure 6.11) and longer, so that statistical methods are no longer fully valid, the last row in Table 6.1 is obtained by RSS of the corresponding individual components. The given values contain a large uncertainty mainly because it was not possible to measure the path length sections L1 and L4. Nevertheless, we believe the data indicate that the path length specification is fulfilled.

For time scales of 30 minutes and longer the influence of the daily ambient temperature variation (and irradiation by sunshine) and the associated thermal dilation of the steel parts becomes noticeable. However, as illustrated in Figure 6.12 for the fork arm of the AEC antenna, the path length variations for the steel parts can be predicted with good precision from a relatively small number of temperature measurements (sensors) and calculation of the thermal dilation, either in an empirical way or from a FEM.

The data indicate that the path length specification is fulfilled, certainly for time intervals of 30 minutes and shorter. Other dedicated measurements indicate that the path length specification is also fulfilled for motions of the telscope, *i.e.* sidereal tracking, OTF and fast switching.

6.5.2 Accelerometer Measurements

Path length jitter on timescales of several seconds was determined from the BUS boresight motion with respect to ground, and the differential boresight motion of the subreflector with respect to the BUS. For sidereal tracking and wind effects, path length stability is typically within a few microns over these timescales.

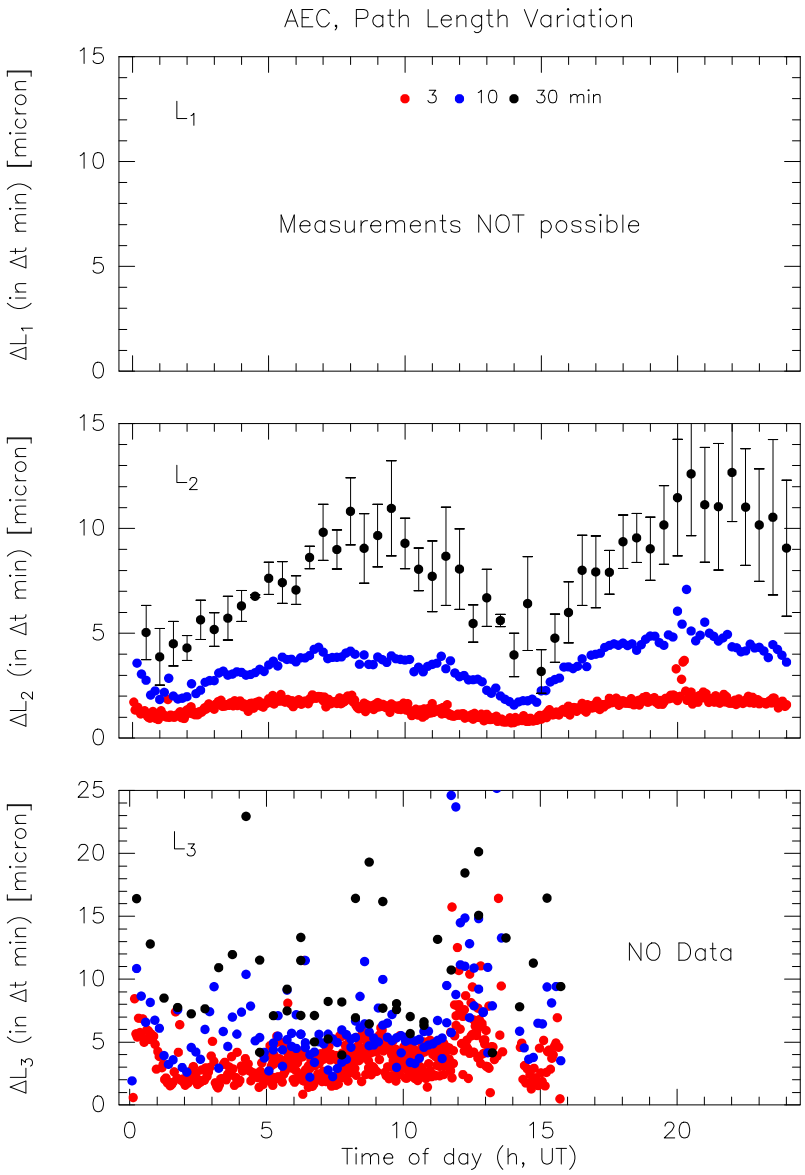

Figure 6.11: Variation of path length L1: pedestal, of path length L2: fork arm, and of path length L3: main reflector vertex to subreflector apex, as a function of the time of the day (UT), and within intervals of 3 minutes (red), 10 minutes (blue), and 30 minutes (black) duration. Note the difference in scale. The error bars are RMS values for a 30 minute time interval. For the displayed values ΔL3, the thermal dilation of the aluminum subreflector support and the support of the API has been eliminated. Local time = UT − 6 hours.

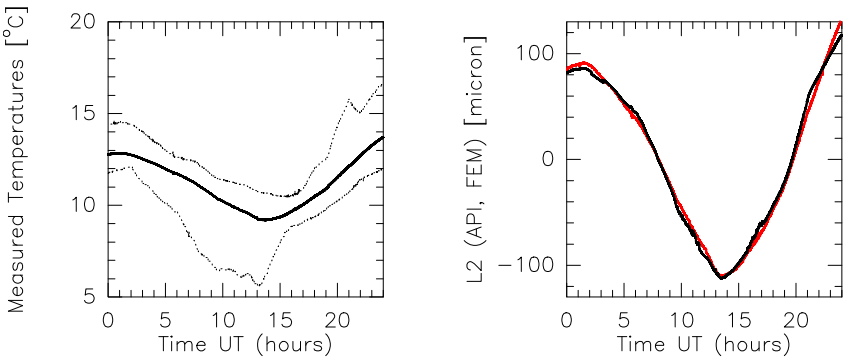

Figure 6.12: Predictability of the long–term path length variation of the steel components from temperature measurements on the AEC antenna, illustrated for the left fork arm on 2003/04/21. Left–side: average temperature of the fork arm derived from 14 temperature sensors: black line; maximum and minimum temperature of fork arm: dashed lines. Right–side: API measured path length variation: black line; path length variation predicted from the corresponding temperature measurements (left–side) used in the FEM: red line.

6.6 Focus Performance

6.6.1 Elevation Dependence

The measured (API, QD) deflections of the BUS and the subreflector support (quadripod) are summarized in Figure 6.13.
Note that:

1. The deflection of the rim of the BUS (panel (a) in Figure 6.13) is very small ($\sim \pm 0.05$ mm), suggesting a stiff BUS. The measurements agree with the prediction from the FEM.

2. The measured droop of the subreflector (sag-y) and the measured shift of the subreflector along the focal axis (sag-z), as a function of elevation, are larger than the prediction from the FEM. This may mean that the quadripod is less stiff than predicted.

3. The radiometric measurements also deliver data on the change in focus. In this case, the measurements reflect the change as a result of both a variation of elevation angle and in ambient temperature. The data have been analysed to yield the change in focus position as functions of these two variables individually. The following expression represents the change in axial focus position:

$$\mathrm{Z-focus(mm)} = 0.977 \sin(El) + 0.020T(C) + 5.646.$$

The results of the measurements are summarised in Figure 6.13.

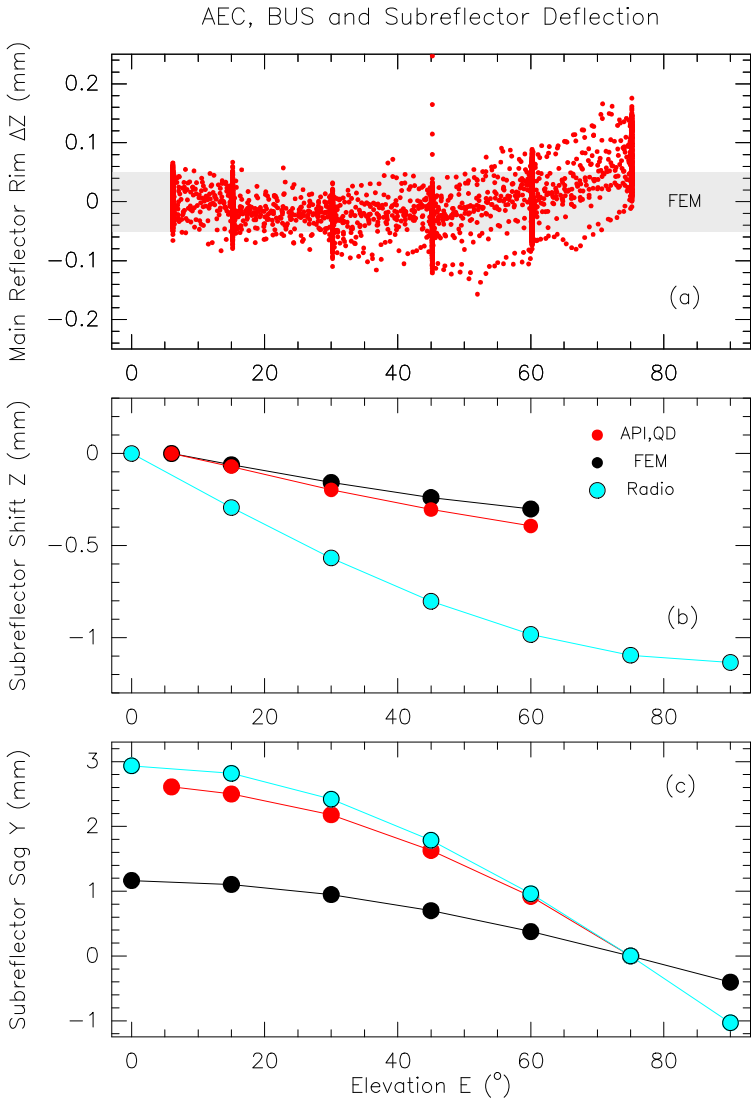

Figure 6.13: Mechanical (API,QD) and radio measurements of the BUS deflection and subreflector (quadripod) deflection, as a function of elevation, and compared to FEM calculations. (a) Change of main reflector rim, in z-direction (direction focus) as measured from the vertex. [The change in focal length is approximately 2 times the plotted value]. The data are obtained by moving the antenna up and down in elevation. (b) Change of distance between vertex and subreflector apex (mechanical measurement) and required change in focal length (radio measurements). (c) sag of subreflector in vertical direction (sag Y), and radiometrically required Y translation of the subreflector.

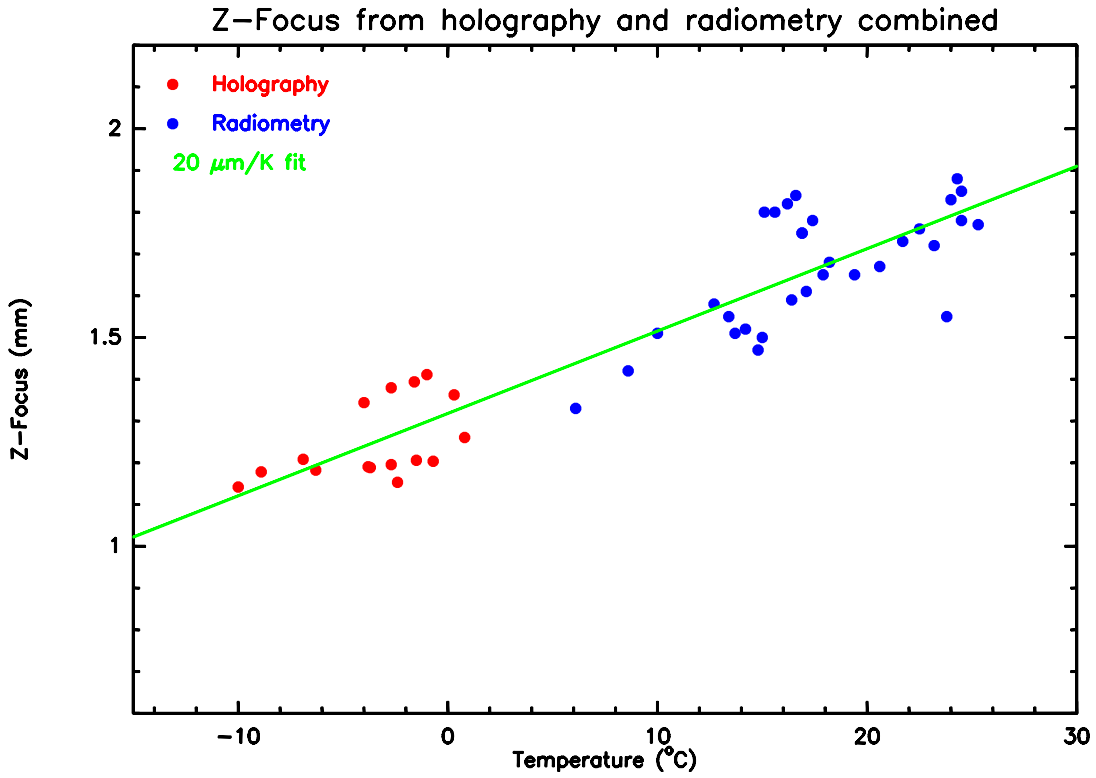

Figure 6.14: The change in focal length as a function of the ambient temperature derived from radiometer and holography measurements. The linear fit gives 20μm/C change.

6.6.2 Temperature Dependence

From the radiometer and holography measurements we have derived the change in best–fit focal length of the primary reflector as a function of temperature. From holography maps alone, spanning an ambient temperature range from -10 to $+3$ C, the focal length indicates a linear change of 15 μm/C. As shown in the formula above, the radiometer measurements show a change of 20 μm/C over a temperature range of 6 to 25 C. All measurements with a common linear fit are shown in Figure 6.14

Appendix A

Acronym Dictionary

AEC: Alcatel EIE Consortium

AEG: Antenna Evaluation Group

ALMA: Atacama Large Millimeter Array

API: Automated Precision Incorporated

ATF: ALMA Test Facility

AUI: Associated Universities Incorporated

BUS: Back-Up Structure

CAN: Controller Area Network

CFRP: Carbon Fibre Reinforced Plastic

DOF: Degrees of Freedom

EKH: Emerson, Klein, and Haslam

ESO: European Southern Observatory

FEM: Finite Element Model

GFRP: Glass Fibre Reinforced Plastic

MOTF: Mosaic (or interferometric) On-The-Fly

NRAO: National Radio Astronomy Observatory

HIA: Herzberg Institute for Astrophysics

IRAM: Institut de Radioastronomie Millimétrique

OAN: Observatorio Astronómico Nacional

OPT: Optical Pointing Telescope

OTF: On-The-Fly

QD: Quadrant Detector

RAL: Rutherford Appleton Laboratory

RMS: Root Mean Square

RSS: Root Sum Square

TPOTF: Total Power (or single dish) On-The-Fly

VLA: Very Large Array